J. Mech. Phys. Solids 186 (2024) 105558

Contents lists available at ScienceDirect

Journal of the Mechanics and Physics of Solids

journal homepage: www.elsevier.com/locate/jmps

Effective surface forces and non-coherent interfaces within the reduced relaxed micromorphic modeling of finite-size mechanical metamaterials

Leonardo A. Perez Ramirez [a,*], Félix Erel-Demore [a], Gianluca Rizzi [a], Jendrik Voss [a], Angela Madeo [b]

[a] Faculty of Architecture and Civil Engineering, TU Dortmund, August-Schmidt-Str. 8, Dortmund, Germany
[b] Head of Chair of Continuum Mechanics, Faculty of Architecture and Civil Engineering, TU Dortmund, August-Schmidt-Str. 8, Dortmund, Germany

ARTICLE INFO

Keywords:
Finite-size metamaterials
Reduced relaxed micromorphic model
Imperfect interfaces
Enriched continuum mechanics
Microstructures

ABSTRACT

This paper introduces for the first time the concepts of non-coherent interfaces and microstructure-driven interface forces in the framework of micromorphic elasticity. It is shown that such concepts are of paramount importance when studying the response of finite-size mechanical metamaterials at the homogenized macro-scale. The need of introducing interface forces is elucidated through numerical examples comparing reduced relaxed micromorphic simulations to their full-microstructured counterparts. These results provide a milestone for the understanding of metamaterials' modeling at the homogenized scale and for the use of micromorphic-type models to achieve an accurate upscaling towards larger-scale metamaterials' structures.

1. Introduction

As it is well known, surfaces of bodies and interfaces between pairs of bodies exhibit properties quite different from those associated with their bulk, due to the fact that molecules or other small-scale heterogeneities result to have different arrangements in proximity of the material's boundaries than when they are forming a 3D network embedded in the material's bulk (Adam, 1941; Adamson and Gast, 1967; Gurtin and Ian Murdoch, 1975). This statement becomes even more true when considering so-called metamaterials, since the heterogeneities that come into play have characteristic sizes of many orders of magnitude bigger than typical molecules' sizes and thus have greater chances to affect the macroscopic material behavior (both in the bulk and in proximity of interfaces) at those large scales that are familiar to engineers.

Metamaterials (from the Greek "meta" = beyond) are materials with architectured microstructures in which the mechanical properties of the microscopic components (unit cells) have an important effect at the macroscopic scale. These metamaterials are often engineered by means of the periodic repetition in space of so-called unit cells that are designed to show special deformation mechanisms triggering exotic mechanical responses at the macroscopic scale. In other words, the mechanical and geometrical properties of metamaterials' microstructure are designed so that they strongly affect the overall bulk metamaterial properties. Typical examples are metamaterials exhibiting band-gaps (frequency ranges in which elastic waves cannot propagate) (Bilal et al., 2018; Celli et al., 2019; El Sherbiny and Placidi, 2018; Goh and Kallivokas, 2019; Koutsianitis et al., 2019; Liu et al., 2000; Wang et al., 2014; Zhu et al., 2015; Fedele et al., 2023), cloaking (elastic waves proceed unperturbed even if hitting the metamaterial) (Bückmann

* Corresponding author.
E-mail address: leonardo.perez@tu-dortmund.de (L.A. Perez Ramirez).

https://doi.org/10.1016/j.jmps.2024.105558
Received 21 December 2023; Received in revised form 23 January 2024; Accepted 27 January 2024
Available online 2 February 2024

et al., 2015; Misseroni et al., 2019, 2016; Norris et al., 2014; Rossi et al., 2020), focusing (a diffused incident wave is focused in a ray while passing inside the metamaterial) (Cummer et al., 2016; Guenneau et al., 2007), channeling (elastic waves take patterns with specific orientations while passing into the metamaterial) (Bordiga et al., 2019; Kaina et al., 2017; Miniaci et al., 2019; Tallarico et al., 2017; Wang et al., 2018), negative refraction (waves are reflected in unusual ways when hitting an interface) (Bordiga et al., 2019; Lustig et al., 2019; Morini et al., 2019; Srivastava, 2016; Willis, 2016; Zhu et al., 2015), and many others, both in the static and dynamic regime.

In the last decades, many homogenization techniques have emerged trying to establish how to derive suitable macroscopic PDEs for mechanical metamaterials starting from specific microscopic unit-cells (Allaire, 1992; Andrianov et al., 2008; Auriault and Boutin, 2012; Bensoussan et al., 2011; Boutin et al., 2014; Chen and Fish, 2001; Craster et al., 2010; Marigo and Maurel, 2016; Touboul et al., 2020; Willis, 2011, 2012). However, since the target macroscopic model is generally chosen a priori to depend only on the displacement field (classical elasticity), the associated parameters (mass and/or stiffness) turn out to be frequency-dependent and may become negative for frequencies approaching the resonance frequency of the internal mass.

Recently, so-called computational homogenization techniques have been proposed that complement these upscaling techniques to include the possibility of letting enriched continua of the micromorphic type emerge at the macroscopic scale (Liu et al., 2021; Sridhar et al., 2016). In the last 50 years countless efforts have been deployed to develop reliable effective models for the description of heterogeneous materials. This has mainly been done in view of the tremendous advantage that a reliable effective model would bring in terms of new possibilities for meta-structural design at the large scales which are relevant for engineers (it is well known that fully microstructured simulations become unaffordable in terms of computational costs already for relatively few unit cells). However, only very few authors seem to be aware of the crucial role that interface forces must play to develop realistic effective models for metamaterials.

Even if it is quite evident that interfaces at metamaterials' boundaries must play a predominant role in the mechanical response of finite-size metamaterials, this issue is often disregarded, due to the complexity of adapting classical homogenization techniques to media with boundaries. Indeed, using classical homogenization methods in realistic bounded domains is an issue which is an open scientific challenge (Cornaggia and Lombard, 2023). Oscillating layers appearing near to interfaces can be accounted for in homogenization techniques by using corrector functions (Moskow and Vogelius, 1997; Josien, 2019; Cakoni et al., 2016, 2019; Vinoles, 2019). However, these boundary correctors are complex objects that make difficult a thorough theoretical study (Armstrong et al., 2017; Gérard-Varet and Masmoudi, 2012) and their direct computation is often as costly as the one of the original problem defined on the microstructured domain (Cornaggia and Lombard, 2023). Few works address the ≪ practical implementation ≫ of these correctors in view of possible numerical implementation and simulation (Beneteau, 2021; Vinoles, 2019, 2016; Marigo and Maurel, 2017; Maurel and Marigo, 2018). The time domain simulation of such homogenized models with boundaries is even more challenging and almost inexistent except for few noticeable examples (Cornaggia and Lombard, 2023; Beneteau, 2021). To deal with such complexity, in the present work, we adopt a different perspective with respect to bottom-up homogenization techniques and we postulate our problem directly at the macro-scale. Leveraging the reduced relaxed micromorphic model that largely showed its performances for the description of metamaterials' bulk propagation problems at the macro-scale (Demore et al., 2022; Demetriou et al., 2023), we complement it with the possibility of macroscopic traction discontinuities at the considered macroscopic boundaries, which take the form of ≪ interface forces ≫. Refraining from trying to obtain a general expression of these interface forces via a bottom-up approach (given the aforementioned difficulties), we explore the nature of such macroscopic interface forces based on a phenomenological approach. In other words, we postulate the expression of such macroscopic interface forces based on (i) a comparison with the corresponding microstructured force and (ii) a comparison with the effect of such interface force on the reduced relaxed micromorphic solution for the displacement field. We show that our procedure is able to bring new answers concerning the numerical implementation and simulation of realistic bounded metamaterials' domains and that it opens new perspectives to inspire the target boundary forces that should be looked for by bottom-up homogenization approaches.

It is intuitively clear that if the metamaterials' micro-heterogeneities are so pronounced that they have a tangible effect on the macroscopic metamaterials' bulk response, they will have even more weight when considering macroscopic metamaterials' interfaces that naturally occur when considering finite-size problems instead of infinite size domains. It can be stated that such interface effects will play a greater role when decreasing the size of the considered macroscopic specimen.

It has been largely shown that the bulk mechanical response of mechanical metamaterials can be effectively explored using an elastic- and inertia-augmented micromorphic model (reduced relaxed micromorphic model) which is able to describe the main metamaterials' fingerprint characteristics (anisotropy, dispersion, band-gaps, size-effects, etc.), while keeping a reduced structure (free of unnecessary parameters) (Aivaliotis et al., 2020; Madeo et al., 2015; Neff et al., 2020, 2015, 2014; Voss et al., 2023; Perez Ramirez et al., 2023; Demetriou et al., 2023; Rizzi et al., 2021; Demore et al., 2022; Rizzi et al., 2022b,c,a). This model can be linked a posteriori to real metamaterials' microstructures via an inverse fitting procedure. The reduced model's structure, coupled with the introduction of well-posed boundary conditions, allowed us to unveil the dynamic response of metamaterials' bricks of finite-size and complex shapes when microstructure-driven interface effects can be considered to be negligible. Indeed, depending on the type of applied load and on the specific micro- and macro-geometry of the problem at hand, interface forces may still have a moderate effect on the overall metamaterial's behavior (Demetriou et al., 2023). However, when considering more complex loading conditions, different unit cells and/or samples of small dimensions, interface effects can no longer be ignored and the reduced relaxed micromorphic model must be enhanced to account for these effects.

In the present paper, we address for the first time, the fundamental issue of including interface effects in the reduced relaxed micromorphic framework by generalizing the typical interface models that can be found in the literature for classical elasticity.

Classical interface models can be divided into different classes based on continuity of certain variables associated with the problem at hand, namely the displacement and the traction at the considered interface. In particular, the most common interface models can be briefly reviewed as follows:

- *Perfect interfaces.* Both the displacement and the traction are continuous across a perfect interface (Javili et al., 2017; Spannraft et al., 2022; Firooz et al., 2021; Perez Ramirez et al., 2023; Demetriou et al., 2023; Rizzi et al., 2021; Demore et al., 2022; Rizzi et al., 2022b,c,a).
- *Cohesive interfaces.* If either the displacement or the traction has a jump across the interface, the interface model is imperfect. A cohesive interface is a particular imperfect interface and allows for displacement jumps across the interface but continuity of the traction is still satisfied (Barenblatt, 1959, 1962; Dugdale, 1960; Needleman, 1987; Xu and Needleman, 1994; Ortiz and Pandolfi, 1999; Charlotte et al., 2006; Alfano and Crisfield, 2001; Gasser and Holzapfel, 2003; van den Bosch et al., 2006; Fagerström and Larsson, 2006; Park et al., 2009; Mosler and Scheider, 2011; Park and Paulino, 2011; Dimitri et al., 2015).
- *Elastic interfaces.* Contrarily to the cohesive interface model, the displacement is continuous across an elastic interface but the traction is discontinuous (Murdoch, 1976; Moeckel, 1975; dell'Isola and Romano, 1987; Fried and Gurtin, 2007; Gurtin and Ian Murdoch, 1975).
- *General interfaces.* Those interfaces allow both jumps in the displacement and the traction (Javili et al., 2017; Bövik, 1994; Hashin, 2002; Benveniste and Miloh, 2001; Monchiet and Bonnet, 2010; Benveniste, 2013).

In the present paper we will only focus on the generalization of the concept of elastic interfaces in the context of micromorphic elasticity, because the considered metamaterials' interfaces are always such that the macroscopic displacement remains continuous due to fast bonding of the solid phases across the interface. However, the presence of voids inside the unit cells implies that the considered interfaces may also contain empty spaces on one or both sides, so that the traction can be expected to suffer jumps across these interfaces.

While the concept of ≪ interface models ≫ is well known in classical elasticity interface problems, their use is always limited to treat interfaces induced by damage (Spannraft et al., 2022; Barenblatt, 1959, 1962; Dugdale, 1960), adhesives between two different media (Spannraft et al., 2022; Klarbring, 1991; Klarbring and Movchan, 1998; Geymonat et al., 1999; Xu et al., 2003; Zhang and Wang, 2009; Alfano et al., 2009; Mubashar et al., 2011; Campilho et al., 2013), surface effects in nano-systems (Sharma and Ganti, 2004; Sharma and Wheeler, 2007; Sharma et al., 2003), fracture (Shih and Ebert, 1987; Tvergaard and Hutchinson, 1993; Wei and Hutchinson, 1999; Park et al., 2009; Chandra, 2002; Li et al., 2005; Sun and Jin, 2006; Park and Paulino, 2011), delamination (Espinosa et al., 2000; Hu et al., 2008; Aymerich et al., 2008; Liu and Islam, 2013; Parrinello et al., 2016; Reinoso et al., 2017), crack growth (England, 1966; Tvergaard and Hutchinson, 1996; Yang et al., 2001; Roe and Siegmund, 2003; Bouvard et al., 2009; Kawashita and Hallett, 2012), bond failure (Ingraffea et al., 1984; Huang and Korobeinik, 2001), screw dislocations (Fan and Wang, 2003), grain boundaries (Mori and Mura, 1987; Pezzotta et al., 2008; Wulfinghoff, 2017), peeling (Wei and Hutchinson, 1998). No applications to mechanical metamaterials can be found until today.

When more theoretical studies are considered, the concept of ≪ interface models ≫ is almost always applied to infinite-size periodic structures obtained by the repetition in space of specific unit cells. Those interfaces are always assumed to occur at the microscopic scale, namely, at the interface between two phases inside the unit cell (Firooz et al., 2021; Needleman, 1987; Mogilevskaya et al., 2008; Chatzigeorgiou et al., 2017; Alfano and Crisfield, 2001; Shuttleworth, 1950; Sharma et al., 2003; Dingreville et al., 2005; Duan et al., 2005; Benveniste and Miloh, 2001; Hashin, 2002; Chen et al., 2006; Javili et al., 2013): homogenization techniques are then applied to show that these non-perfect interfaces at the micro-level produce scale effects (elastic properties of the homogenized composite that depend on the size of the base unit cell) (Javili et al., 2017; Ottosen et al., 2016; Firooz et al., 2021; Javili et al., 2015; Ban and Mi, 2020; Yang, 2004; Yvonnet et al., 2008; Dingreville et al., 2014; Chen and Pindera, 2020; Sharma, 2004; Zemlyanova and Mogilevskaya, 2018; Le, 2020). To the authors' knowledge, there is no study that considers generalized interfaces to model macroscopic metamaterials' boundaries, interfaces between different metamaterials or between metamaterials and classical homogeneous materials. When we talk about macroscopic interfaces, we mean that we consider a finite block of a given metamaterial which can be connected to another metamaterial block or to a block of homogeneous material: those interfaces can then be seen as composed by a finite number of unit cells which confer specific elastic properties to the interface itself. Macroscopic interface forces can be activated at those macroscopic interfaces, due to the heterogeneity of the underlying microstructure at the lower scales. The present paper will address this issue for the first time and will open new perspectives for future studies.

The paper is organized as follows:

In Section 1 we address the fundamental issue of "interface forces" occurring in the continuum modeling of mechanical metamaterials and we frame it in the context of the existing state of the art. Section 2 is devoted to the generalization of the concept of "elastic interface" in the context of reduced relaxed micromorphic elasticity. In particular, we show how to deal with these surface forces occurring at (i) free micromorphic boundaries as a result of the presence of an underlying microstructure and (ii) at interfaces separating two reduced relaxed micromorphic media or a reduced relaxed micromorphic medium from a homogeneous material. In Section 3, we show how to use the novel concept of reduced relaxed micromorphic interface forces to model free metamaterials' interfaces, and interfaces arising between two metamaterials or a metamaterial and a homogeneous material. In Section 4 we start unveiling the efficacy of the concept of reduced relaxed micromorphic interface forces with a specific example in which two different metamaterial's interfaces are generated by using two different "unit cell's cuts" stemming from the same bulk metamaterial. In Section 5 we further explore the efficacy of the new continuum modeling framework through a more

complex numerical example involving interfaces between a metamaterial and a homogeneous material. Section 6 finally provides the conclusions about our findings and the multiple perspectives which are now open to drive the theoretical investigations about surface forces in the framework of reduced relaxed micromorphic elasticity towards tangible large-scale applications involving finite-size metamaterials as base building blocks.

2. Equations of motion and boundary conditions for the reduced relaxed micromorphic model

2.1. Bulk equations and "free interface" boundary conditions

The kinetic energy K and strain energy W of the reduced relaxed micromorphic model are shown in Eqs. (1)–(2) (Demetriou et al., 2023; Rizzi et al., 2021; Perez Ramirez et al., 2023; Voss et al., 2023):

$$\begin{aligned} K\left(\dot{u},\nabla\dot{u},\dot{P}\right) =& \frac{1}{2}\rho\,\langle\dot{u},\dot{u}\rangle + \frac{1}{2}\langle\mathbb{J}_{\mathrm{m}}\,\mathrm{sym}\,\dot{P},\mathrm{sym}\,\dot{P}\rangle + \frac{1}{2}\langle\mathbb{J}_{\mathrm{c}}\,\mathrm{skew}\,\dot{P},\mathrm{skew}\,\dot{P}\rangle \\ &+ \frac{1}{2}\langle\mathbb{T}_{\mathrm{e}}\,\mathrm{sym}\nabla\dot{u},\mathrm{sym}\nabla\dot{u}\rangle + \frac{1}{2}\langle\mathbb{T}_{\mathrm{c}}\,\mathrm{skew}\nabla\dot{u},\mathrm{skew}\nabla\dot{u}\rangle\ , \end{aligned} \tag{1}$$

$$\begin{aligned} W\left(\nabla u,P\right) =& \frac{1}{2}\langle\mathbb{C}_{\mathrm{e}}\,\mathrm{sym}\left(\nabla u-\ P\right),\mathrm{sym}\left(\nabla u-\ P\right)\rangle \\ &+ \frac{1}{2}\langle\mathbb{C}_{\mathrm{c}}\,\mathrm{skew}\left(\nabla u-\ P\right),\mathrm{skew}\left(\nabla u-\ P\right)\rangle \\ &+ \frac{1}{2}\langle\mathbb{C}_{\mathrm{micro}}\,\mathrm{sym}\,P,\mathrm{sym}\,P\rangle\ . \end{aligned} \tag{2}$$

The Lagrangian density can thus be written as:

$$\mathcal{L}\ :=\ K\left(\dot{u},\nabla\dot{u},\dot{P}\right) - W\left(\nabla u,P\right)\ . \tag{3}$$

In the previous formulas, $u\in\mathbb{R}^3$ is the macroscopic displacement field, $P\in\mathbb{R}^{3\times3}$ is the non-symmetric micro-distortion tensor, ρ is the macroscopic apparent density, $\mathbb{J}_{\mathrm{m}}$, $\mathbb{J}_{\mathrm{c}}$, $\mathbb{T}_{\mathrm{e}}$, $\mathbb{T}_{\mathrm{c}}$ are 4th order micro-inertia tensors, and $\mathbb{C}_{\mathrm{e}}$, $\mathbb{C}_{\mathrm{m}}$, $\mathbb{C}_{\mathrm{c}}$ are 4th order elasticity tensors. These tensors in Voigt notation, for the tetragonal symmetry case and reporting only the in-plane components, can be expressed as (Aivaliotis et al., 2020; d'Agostino et al., 2020):[1]

$$\begin{aligned} \mathbb{C}_{\mathrm{e}} &= \begin{pmatrix} \kappa_{\mathrm{e}}+\mu_{\mathrm{e}} & \kappa_{\mathrm{e}}-\mu_{\mathrm{e}} & \star & \dots & 0\\ \kappa_{\mathrm{e}}-\mu_{\mathrm{e}} & \kappa_{\mathrm{e}}+\mu_{\mathrm{e}} & \star & \dots & 0\\ \star & \star & \star & \dots & 0\\ \vdots & \vdots & \vdots & \ddots & \\ 0 & 0 & 0 & & \mu_{\mathrm{e}}^{*} \end{pmatrix}, \qquad \mathbb{C}_{\mathrm{micro}} = \begin{pmatrix} \kappa_{\mathrm{m}}+\mu_{\mathrm{m}} & \kappa_{\mathrm{m}}-\mu_{\mathrm{m}} & \star & \dots & 0\\ \kappa_{\mathrm{m}}-\mu_{\mathrm{m}} & \kappa_{\mathrm{m}}+\mu_{\mathrm{m}} & \star & \dots & 0\\ \star & \star & \star & \dots & 0\\ \vdots & \vdots & \vdots & \ddots & \\ 0 & 0 & 0 & & \mu_{\mathrm{m}}^{*} \end{pmatrix}, \\ \mathbb{J}_{\mathrm{m}} &= \rho L_{\mathrm{c}}^{2}\begin{pmatrix} \kappa_{\gamma}+\gamma_{1} & \kappa_{\gamma}-\gamma_{1} & \star & \dots & 0\\ \kappa_{\gamma}-\gamma_{1} & \kappa_{\gamma}+\gamma_{1} & \star & \dots & 0\\ \star & \star & \star & \dots & 0\\ \vdots & \vdots & \vdots & \ddots & \\ 0 & 0 & 0 & & \gamma_{1}^{*} \end{pmatrix}, \qquad \mathbb{T}_{\mathrm{e}} = \rho L_{\mathrm{c}}^{2}\begin{pmatrix} \overline{\kappa}_{\gamma}+\overline{\gamma}_{1} & \overline{\kappa}_{\gamma}-\overline{\gamma}_{1} & \star & \dots & 0\\ \overline{\kappa}_{\gamma}-\overline{\gamma}_{1} & \overline{\kappa}_{\gamma}+\overline{\gamma}_{1} & \star & \dots & 0\\ \star & \star & \star & \dots & 0\\ \vdots & \vdots & \vdots & \ddots & \\ 0 & 0 & 0 & & \overline{\gamma}_{1}^{*} \end{pmatrix}, \\ \mathbb{J}_{\mathrm{c}} &= \rho L_{\mathrm{c}}^{2}\begin{pmatrix} \star & 0 & 0\\ 0 & \star & 0\\ 0 & 0 & 4\gamma_{2} \end{pmatrix}, \qquad \mathbb{T}_{\mathrm{c}} = \rho L_{\mathrm{c}}^{2}\begin{pmatrix} \star & 0 & 0\\ 0 & \star & 0\\ 0 & 0 & 4\overline{\gamma}_{2} \end{pmatrix}, \qquad \mathbb{C}_{\mathrm{c}} = \begin{pmatrix} \star & 0 & 0\\ 0 & \star & 0\\ 0 & 0 & 4\mu_{\mathrm{c}} \end{pmatrix}. \end{aligned} \tag{4}$$

The action functional $\mathcal{A}$ of the micromorphic continuum is defined by:

$$\mathcal{A} = \iint_{\Omega\times[0,T]} \mathcal{L}\left(\nabla u,\dot{u},\nabla\dot{u},P,\dot{P}\right)\,dx\,dt\,, \tag{5}$$

and it operates on a domain Ω over the time interval $[0,T]$. If we consider a conservative system, the work of internal actions corresponds to $\mathcal{W}^{int}\ :=\ \partial\mathcal{A}$, here the variation operator δ operates on the kinematic fields (u,P). If no external forces act on the considered system, an equilibrium condition is found when the first variation of the action functional is equal to zero, $\partial\mathcal{A}=0$. This, in turn, implies the strong form equilibrium equations:

$$\rho\,\ddot{u} - \mathrm{Div}\widehat{\sigma} = \mathrm{Div}\widetilde{\sigma} \qquad \text{and} \qquad \overline{\sigma} = \widetilde{\sigma} - s \qquad \text{in} \quad \Omega\,, \tag{6}$$

together with the boundary conditions:

[1] Where in Aivaliotis et al. (2020), d'Agostino et al. (2020) $\kappa_i=\lambda_i+\mu_i$ with $i=\{e,m\}$, $\kappa_\gamma=\gamma_3+\gamma_1$, $\overline{\kappa}_\gamma=\overline{\gamma}_3+\overline{\gamma}_1$, and $\eta_i=\rho L_c^2\gamma_i$.

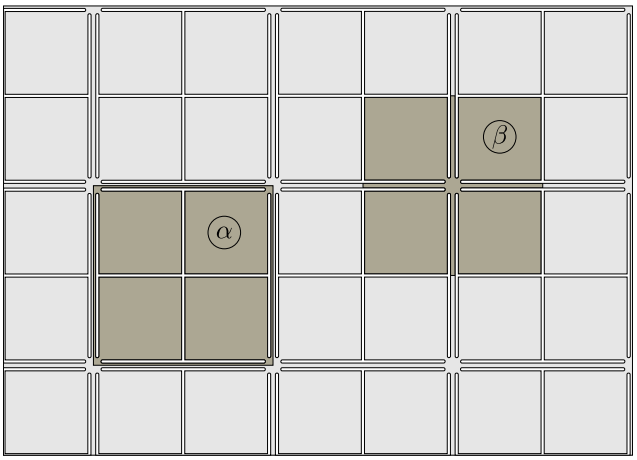

Fig. 1. Two possible unit cell's cuts giving rise to the same metamaterial: α and β cell's cuts.

Generalized traction / displacement boundary conditions at a reduced relaxed micromorphic free interface

$$\underbrace{t := \left(\widetilde{\sigma} + \widehat{\sigma}\right) n = 0}_{\text{vanishing generalized traction}} \quad \text{or} \quad \underbrace{u = \overline{u}}_{\text{assigned displacement}} \quad \text{on} \quad \partial\Omega\,. \tag{7}$$

In the previous formulas, we set:

$$\widetilde{\sigma} := \mathbb{C}_{\mathrm{e}}\,\mathrm{sym}(\nabla u - P) + \mathbb{C}_{\mathrm{c}}\,\mathrm{skew}(\nabla u - P)\,, \qquad \widehat{\sigma} := \mathbb{T}_{\mathrm{e}}\,\mathrm{sym}\,\nabla\dot{u} + \mathbb{T}_{\mathrm{c}}\,\mathrm{skew}\,\nabla\dot{u}\,,$$
$$s := \mathbb{C}_{\mathrm{micro}}\,\mathrm{sym}P\,, \qquad \overline{\sigma} := \mathbb{J}_{\mathrm{m}}\,\mathrm{sym}\,\ddot{P} + \mathbb{J}_{\mathrm{c}}\,\mathrm{skew}\,\ddot{P}\,. \tag{8}$$

It is possible to understand that when a metamaterial interface possesses an underlying microstructure, homogenized surface forces can be generated due to the microstructure itself, especially for some frequency ranges (e.g., band-gap regions) and for specific loading conditions. This leads us to modify the traction boundary condition (7) as follows:[2]

Interface force / displacement boundary conditions at a reduced relaxed micromorphic free interface

$$\underbrace{t := \left(\widetilde{\sigma} + \widehat{\sigma}\right) n = f_{\mathrm{interface}}}_{\text{interface force}} \quad \text{or} \quad \underbrace{u = \overline{u}}_{\text{assigned displacement}} \quad \text{on} \quad \partial\Omega\,, \tag{9}$$

where $f_{\mathrm{interface}}$ is a microstructure-driven interface force that may depend on the frequency, on the type of applied load and on the microstructure's geometry close to the interface. In particular, this interface force will depend on the type of unit cell's cut which is chosen for a given metamaterial (see e.g., Figs. 1 and 2).

Contrarily to Eq. $(7)_1$, the interface force boundary conditions introduced in Eq. $(9)_1$ allow us to discriminate between two different unit cell's cuts through the introduction of this interface force $f_{\mathrm{interface}}$, while remaining in the simplified reduced relaxed micromorphic framework (no need to specify the specific microstructures in a FEM implementation). In fact if, on the one hand, the generalized traction t allows us to account for some microstructure-related effects through the introduction of extra terms with respect to classical elasticity, on the other hand, these extra terms come from the metamaterial's bulk behavior encoded in the expression (5) of the action functional. This means that the generalized traction t alone does not allow us to discriminate between two different unit cell's cuts, since the bulk metamaterial generated by the two cuts is the same (see Fig. 1).

The difference between two unit cell's cuts giving rise to the same metamaterial becomes visible only in the vicinity of the macroscopic metamaterial's interfaces (see Figs. 3 and 4): this motivated us to introduce the "interface force" $f_{\mathrm{interface}}$ in Eq. $(9)_1$, which may account for such interface effects. Even if it is not possible to give *"a priori"* a comprehensive expression for $f_{\mathrm{interface}}$, we can state in general that it will depend on (i) the type of unit cell's cut, (ii) the type of applied load, and (iii) the considered frequency. We will provide explicit expressions for $f_{\mathrm{interface}}$ in Section 4, where a specific "free interface" problem is addressed.

[2] The modified form (9) of the boundary conditions (7) can be easily re-formulated in the framework of the principle of virtual works by adding a specific surface contribution involving $f_{\mathrm{interface}}$ to the work of external actions.

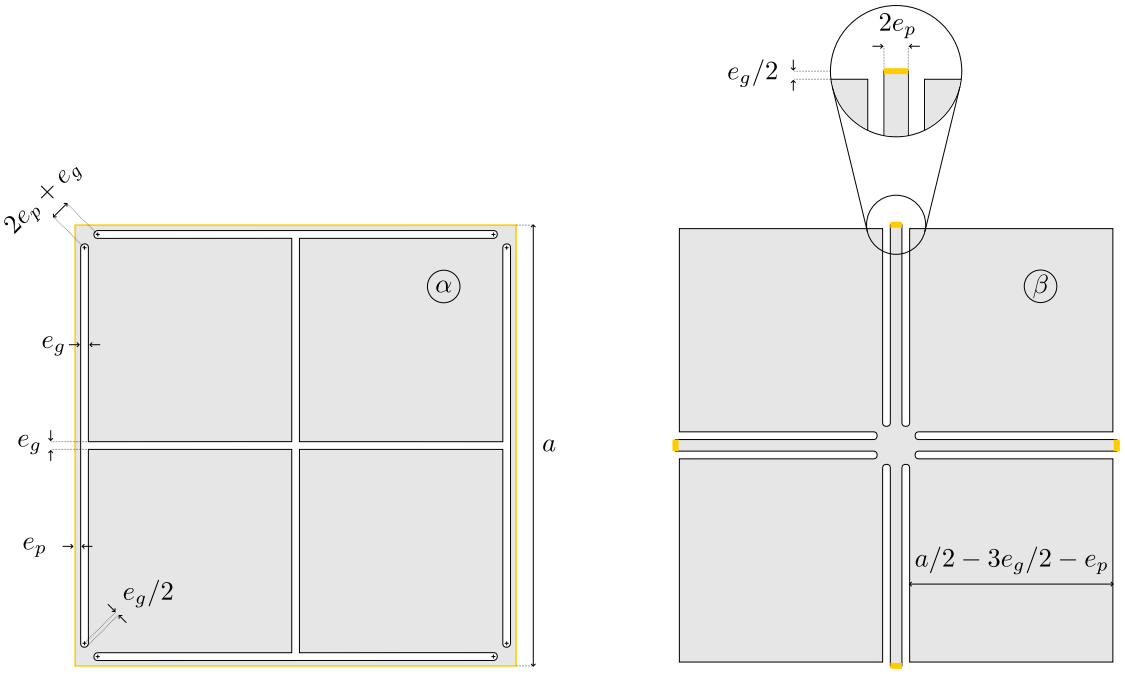

Fig. 2. α and β unit cell's cuts for the metamaterial in Fig. 1. Solid connections are indicated in yellow.

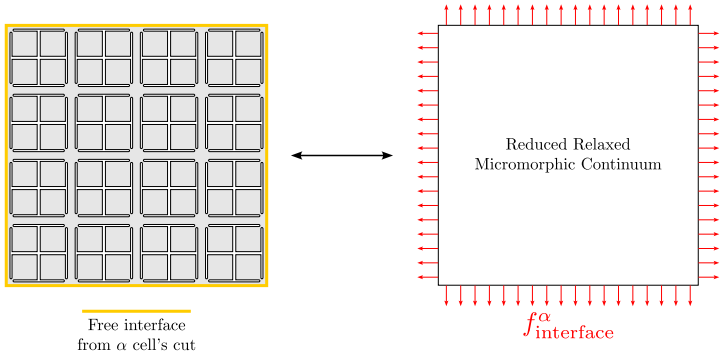

Fig. 3. Free macroscopic metamaterial interface for a metamaterial block stemming from *(left)* the α cell's cut and *(right)* its reduced relaxed micromorphic counterpart, modeled via the introduction of the interface force $f^{\alpha}_{\text{interface}}$.

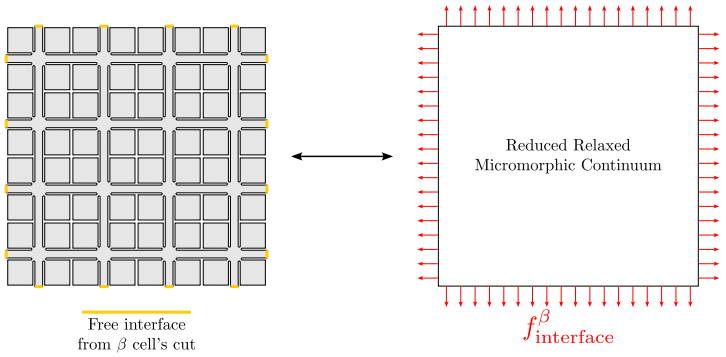

Fig. 4. Free macroscopic metamaterial interface for a metamaterial block stemming from *(left)* the β cell's cut and *(right)* its reduced relaxed micromorphic counterpart, modeled via the introduction of the interface force $f^{\beta}_{\text{interface}}$.

2.2. Interface conditions for coherent and non-coherent reduced relaxed micromorphic interfaces

The interface conditions between two reduced relaxed micromorphic domains Ω^- and Ω^+, which are in contact through a surface Σ, in the absence of external forces, can be derived via the minimization of the action functional $\mathcal{A}$ of Eq. (5), and making use of test functions with compact support including portions of Σ (dell'Isola et al., 2009):

Continuous traction and displacement boundary conditions at a reduced relaxed micromorphic / reduced relaxed micromorphic coherent interface

$$\underbrace{t^+ = t^-}_{\text{continuity of traction}} \quad \text{and} \quad \underbrace{u^+ = u^-}_{\text{continuity of displacement}} . \tag{10}$$

As a particular case, if Ω^+ is a classical isotropic Cauchy continuum, then the interface conditions reduce to

Continuous traction and displacement boundary conditions at a Cauchy / reduced relaxed micromorphic coherent interface

$$\underbrace{t^+_{\text{Cauchy}} = t^-}_{\text{continuity of traction}} \quad \text{and} \quad \underbrace{u^+ = u^-}_{\text{continuity of displacement}} , \tag{11}$$

where $t_{\text{Cauchy}} = \sigma_{\text{Cauchy}} n$, and $\sigma_{\text{Cauchy}} = \lambda \operatorname{tr}(\operatorname{sym}\nabla u)\, \mathbb{1} + 2\mu \operatorname{sym}\nabla u$ is the stress tensor for an isotropic linear elastic material.

Interface conditions for which tractions and displacements are both continuous across the interface are known in classical elasticity as "coherent interfaces" (see Javili et al., 2017; Spannraft et al., 2022; Firooz et al., 2021). We will keep this nomenclature in the generalized framework of micromorphic elasticity.

As already remarked before for the "free interface" conditions, the continuity of generalized tractions given in Eqs. $(10)_1$ (or $(11)_1$) accounts for the fact that the considered (macro-)material possesses an underlying microstructure via the introduction of a generalized traction force containing additional terms with respect to classical Cauchy elasticity (see definitions of $\widetilde{\sigma}$ and $\widehat{\sigma}$ in Eq. (8)). However, these additional terms only account for those microstructure-related effects which come from the bulk and do not allow to discriminate between two different unit cell's cuts in the vicinity of interfaces. With an analogous reasoning as the one drawn in Section 2.1, we modify Eqs. (10), (11) as follows, in order to account for the presence of interface forces directly driven by different unit cell's cuts:

Reduced relaxed micromorphic / reduced relaxed micromorphic elastic (non-coherent) interface

$$\underbrace{[\![t]\!] := t^+ - t^- = f \neq 0}_{\text{jump of traction}} \quad \text{and} \quad \underbrace{u^+ = u^-}_{\text{continuity of displacement}} , \quad f : \begin{array}{l} \partial\Omega \times \mathbb{R}_+ \to \mathbb{R}^3 \\ x, \omega \mapsto f(x, \omega) \end{array} , \tag{12}$$

and

Cauchy / reduced relaxed micromorphic elastic (non-coherent) interface

$$\underbrace{[\![t]\!] := t^+_{\text{Cauchy}} - t^- = f \neq 0}_{\text{jump of traction}} \quad \text{and} \quad \underbrace{u^+ = u^-}_{\text{continuity of displacement}} , \quad f : \begin{array}{l} \partial\Omega \times \mathbb{R}_+ \to \mathbb{R}^3 \\ x, \omega \mapsto f(x, \omega) \end{array} . \tag{13}$$

This modification of the micromorphic traction boundary conditions generalizes what is known in the literature as "boundary conditions for non-coherent interfaces" for the case of classical elasticity (see Javili et al., 2017; Ottosen et al., 2016). Non-coherent interfaces can be found between two materials that are non-homogeneous close to the considered interface due to the presence of voids or defects. The different possible cases that are possible in a "continuum mechanics" framework to describe non-coherent interfaces, are those allowing jumps of tractions but not displacement jumps (elastic interfaces), those allowing displacement jumps but not traction jumps (cohesive interfaces), and those allowing both traction and displacement jumps (general interfaces) (see Javili et al., 2017 and Section 1).

Given the specific characteristics of the materials considered in this paper, it is clear that, since the two media are always strongly connected at the considered interfaces, the macroscopic displacement jump must be considered to be vanishing (continuity of macroscopic displacement). On the other hand, given the presence of voids in the vicinity of the considered interfaces, the jump of traction can be non-vanishing. In this work, we will thus limit ourselves to generalize only elastic (non-coherent) interface conditions in the framework of micromorphic elasticity. It is worth to explicitly remark that imposing non-vanishing traction jumps turns out to be equivalent to the existence of a microstructure-related surface force as in the "free interface" case considered in Section 2.1.

Table 1
Geometrical and elastic parameters of the metamaterial's unit cell.

a [mm]	e_g [mm]	e_p [mm]	ρ_{Ti} [kg/m^3]	λ_{Ti} [GPa]	μ_{Ti} [GPa]
20	0.35	0.25	4400	88.8	41.8

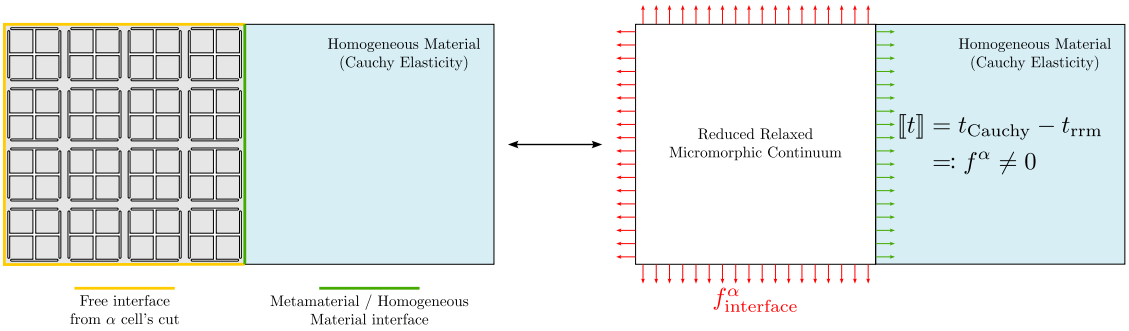

Fig. 5. *(Left)* Metamaterial interface *(green line)* between a metamaterial stemming from the unit cell cut α and a homogeneous material and *(right)* its reduced relaxed micromorphic counterpart modeled through the introduction of a non-vanishing traction jump.

3. Interfaces in mechanical metamaterials

The elastic interface conditions newly introduced in Eqs. (9)–(11) allow us to treat, for the first time in the literature, complex interface problems for finite-size metamaterials' structures, in the macroscopic framework of (reduced relaxed) micromorphic elasticity. Indeed, while the concept of "non-coherent interfaces" is well known in classical elasticity interface problems, it has never been used neither to explore complex macroscopic interfaces in mechanical metamaterials, nor to enhance the performances of micromorphic-type continuum models with respect to an effective description of metamaterials' interfaces (see Section 1 for a thorough review of "non-coherent interfaces" and their typical application fields).

In order to provide a concrete example of how elastic interfaces should be implemented in a reduced relaxed micromorphic framework to describe complex problems arising at metamaterials' interfaces, we consider here a metamaterial stemming from the periodic repetition in space of the unit cell presented in Demore et al. (2022) (see Fig. 1).

The unit cell's cuts α and β are two possible extremes allowing to build the metamaterial in Fig. 1, while keeping the tetragonal symmetry: unit cell α provides an interface which is everywhere solid (even if voids are close to the boundary), while unit cell β provides an interface which is empty "almost everywhere" except for small solid connections given by the four "slender" beams (see Fig. 2).

It is clear that many other different cell's cuts with tetragonal symmetry would be possible that give rise to the same bulk metamaterial. However, those cell's cuts would provide interfaces which are intermediate cases between the α cut (full solid interface) and the β cut (almost empty) interface. The base material of the unit cells in Fig. 2 is titanium, its elastic and geometric properties are given in Table 1.

We want to underline again that in the present paper we are interested in "macroscopic interfaces" which arise as boundaries of finite-size metamaterial's blocks, and not in those micro-interfaces that would arise inside the unit cell if the voids would be filled by a different material. Given the fact that the underlying unit cells contain voids, we suppose that the reduced relaxed micromorphic interfaces will be subjected to macroscopic interface forces (or jump of forces) directly stemming from the heterogeneity of the unit cells which are adjacent to the considered interfaces (see Fig. 3).

This is a quite different approach to "non-coherent interfaces" with respect to the one usually found in the literature, where such generalized interfaces are always considered to arise at the microscopic level, as separation interfaces between two phases inside metamaterial's unit cells (Javili et al., 2017).

When one of our macroscopic interfaces coincides with the boundary of a finite-size metamaterial block, we will call it a "free" metamaterial interface (see Figs. 3 and 4). In the case in which the macroscopic interface separates two metamaterials or a metamaterial from a homogeneous material, we will just call it metamaterial interface (see Figs. 5 and 6). It is clear that different unit cell's cuts (see Fig. 1) will give rise to different macroscopic metamaterial's interfaces and consequently to different interface forces $f_{\mathrm{interface}}$ when passing to the reduced relaxed modeling, see Figs. 3 and 4.

A similar reasoning holds for metamaterial interfaces between two metamaterials or between a metamaterial and a homogeneous material, with the only difference that the interface force has the indirect effect of generating a traction jump across the considered interface. We show in Figs. 5 and 6 the definition of metamaterial's interfaces between a metamaterial and a homogeneous material (the case of an interface between two metamaterials would be completely analogous). In these figures, the homogeneous material is an arbitrary material without voids that follows Cauchy Elasticity.

We have thus set in this section the general framework to treat "free" metamaterial interfaces and metamaterial interfaces between pairs of media in the simplified framework of reduced relaxed micromorphic elasticity. We will show in the following

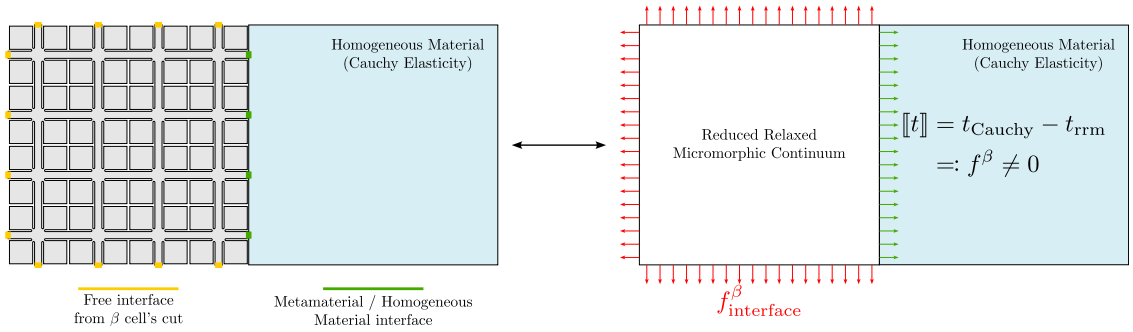

Fig. 6. *(Left)* Metamaterial interface *(green line)* between a metamaterial stemming from the unit cell cut β and a homogeneous material *(left)* and *(right)* its reduced relaxed micromorphic counterpart modeled through the introduction of a non-vanishing traction jump.

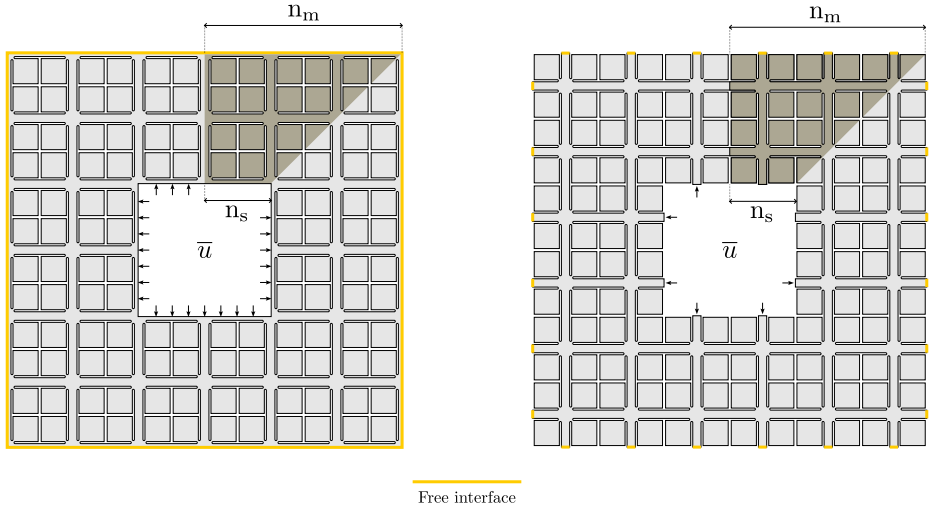

Fig. 7. Full-microstructure setup of the free interface problem for *(left)* α and *(right)* β cell's cuts.

section that, depending on (i) the unit cell cut, (ii) the type of loading and/or (iii) the considered frequency, the effect of the interface forces may become negligible, so that one could simply use the classical reduced relaxed micromorphic modeling where $f_{\text{interface}} = 0$, which implies $[\![t]\!] = 0$. On the other hand, when considering unit cell's cuts which have bigger fractions of voids along the interface and/or specific frequencies (e.g., band-gap frequencies), the correct modeling with $f_{\text{interface}} \neq 0$ and $[\![t]\!] \neq 0$ can no longer be ignored. We will expand these findings in Sections 4 and 5, where specific interface problems are analyzed.

4. Effect of different cell's cuts on a metamaterial's "free interface" problem

We start by implementing in a finite element code, the "free interface" problem defined in Fig. 7, where a metamaterial plate with a central hole is loaded by adding a harmonic radial expansion displacement inside the hole. We use the Structural Mechanics Module of COMSOL Multiphysics® software to perform the simulations (COMSOL). Both the microstructured simulations (α and β cuts) and the reduced relaxed micromorphic simulations are implemented in COMSOL Multiphysics®. To implement the full microstructured simulations we input the detailed geometries and we use the classical elasticity theory to model the mechanical response of the solid phase which is titanium (see Table 1).

In both cases, to reduce computation time, we implement symmetry conditions simplifying the study to the problem in Fig. 8 (see Appendix A.1 for details about the implementation of the symmetry conditions). As for the implementation of the relaxed micromorphic simulations, we implement an analogous continuum domain with boundary conditions (9), as depicted in Fig. 9. Also, in the reduced relaxed micromorphic simulation we implement symmetry conditions as described in Appendix A.1.

To get a first indication of the influence of the interface forces $f_{\text{interface}}$ in the reduced relaxed micromorphic implementation of the problem, we start with the special case in which $f^{\alpha,\beta}_{\text{interface}} = 0$ (which reduces to the simplified conditions of micromorphic free interface given in Eq. (7). Fig. 11 shows the comparison of the norm of the displacement field for different frequencies as obtained from:

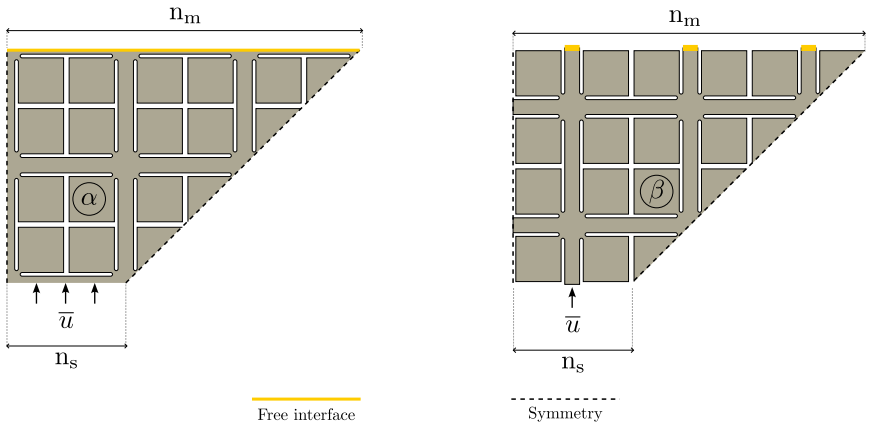

Fig. 8. Symmetrized domain for the *(left)* α and *(right)* β unit cells.

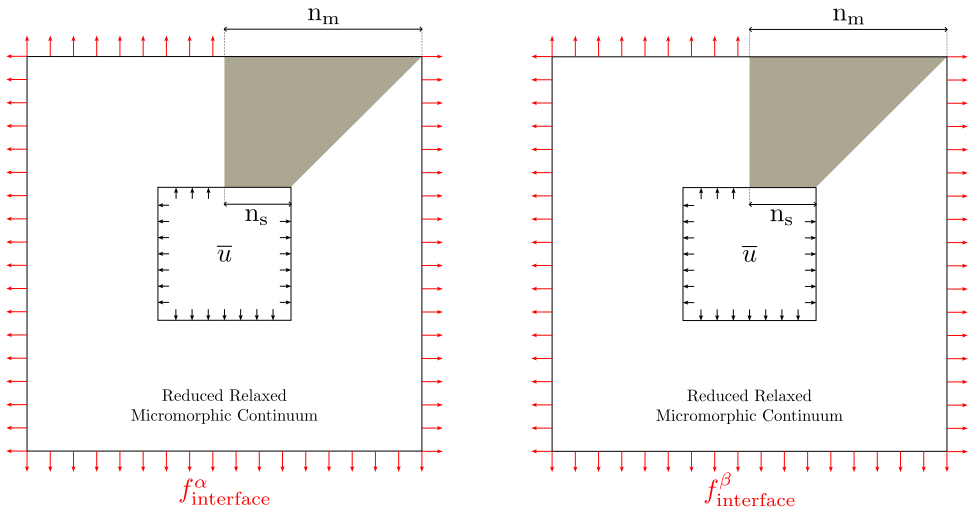

Fig. 9. Reduced relaxed micromorphic formulation of the problem defined in Fig. 7.

- the microstructured problem defined in Fig. 7 (*first column*) β cell's cut, when setting $n_m = 25$, $n_s = 5$ and the radial expansion displacement $\overline{u}_1 = 1 \times 10^{-12} \frac{0.1x}{x^2+y^2}$ [mm], $\overline{u}_2 = 1 \times 10^{-12} \frac{0.1y}{x^2+y^2}$ [mm], $\overline{u}_3 = 0$[mm].
- the microstructured problem defined in Fig. 7 (*second column*) α cell's cut, when setting $n_m = 25$, $n_s = 5$ and the radial expansion displacement $\overline{u}_1 = 1 \times 10^{-12} \frac{0.1x}{x^2+y^2}$ [mm], $\overline{u}_2 = 1 \times 10^{-12} \frac{0.1y}{x^2+y^2}$ [mm], $\overline{u}_3 = 0$[mm].
- the reduced relaxed micromorphic implementation of the problem defined in Fig. 9 when setting $f^{\alpha}_{\text{interface}} = f^{\beta}_{\text{interface}} = 0$ and the radial expansion displacement $\overline{u}_1 = 1 \times 10^{-12} \frac{0.1x}{x^2+y^2}$ [mm], $\overline{u}_2 = 1 \times 10^{-12} \frac{0.1y}{x^2+y^2}$ [mm], $\overline{u}_3 = 0$[mm].
- As a reference case, we also implement a simulation where the metamaterial's domain is simulated by using the long-wave limit of our micromorphic continuum (Barbagallo et al., 2017): a classical Cauchy continuum with tetragonal symmetry whose mechanical properties are given in Table 2.

We can see from Fig. 11 that, overall, the influence of the unit cell's cut on this "free interface" problem is relatively small, since the main small differences (if any) between the macroscopic displacement fields given in the first two columns are mainly concentrated close to the interface where the displacement $\overline{u}$ is applied. The overall displacement pattern is thus very similar in both the α and β cases. This leads us to hypothesize that, apart from a small influence of an interface force that would be eventually activated close to the interface where the displacement is applied, we do not expect the activation of an interface force at the external free interface. The third column in Fig. 11 supports our hypothesis, since the reduced relaxed micromorphic model with vanishing interface forces captures quite well the overall metamaterial's response for the entire range of considered frequencies. From the

Table 2
Parameters of the equivalent tetragonal Cauchy material which is the long-wave limit of the reduced relaxed micromorphic continuum.

λ_{macro} [Pa]	μ_{macro} [Pa]	μ^*_{macro} [Pa]	ρ_{macro} $[\frac{\text{kg}}{\text{m}^3}]$
6.46×10^7	1.61×10^9	1.26×10^6	3975

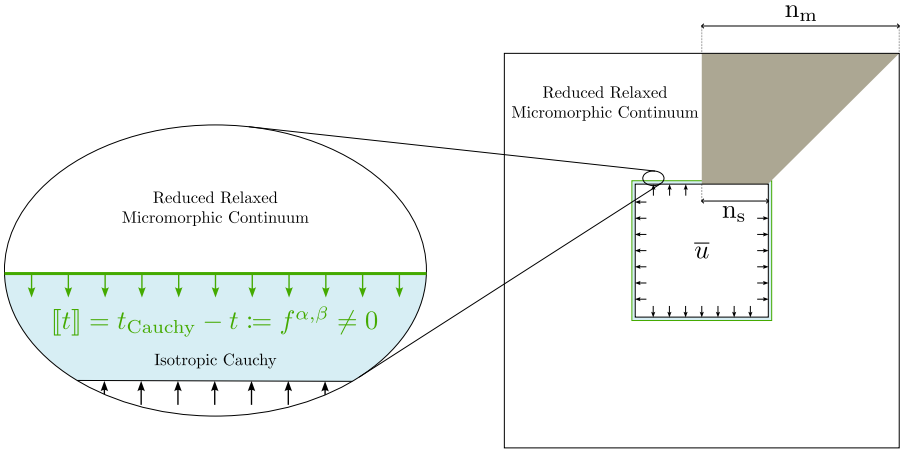

Fig. 10. Reduced relaxed micromorphic implementation of the problem defined in Fig. 7 when a surface force $f^{\alpha,\beta}$ arises close to the loading interface.

fourth column, we can see that, while an anisotropic equivalent Cauchy continuum can capture to a good extent the metamaterial's response at low frequencies, it becomes inadequate when dispersive phenomena start playing a role at higher frequencies. We can also see that for frequencies which are close or belonging to the band-gap region (1400 and 2000 Hz) some quantitative deviations of the reduced relaxed micromorphic model from the microstructured solution can be found, even if the overall qualitative behavior remains well captured. This small deviation leads us to hypothesize that the concentration of the strain across the loading interface, due to the fact that local resonances are activated at those frequencies, would require in the micromorphic simulation that an interface force is activated close to the loading interface in order to correctly describe the complex mechanisms occurring close to band-gap frequencies, see Figs. 13 and 15.[3]

To understand which type of interface force should be applied close to the interface where the displacement has been assigned, we start by analyzing the Cauchy traction issued via the α-cut full-microstructured simulation described in Fig. 8 *(left)*.[4] We then explore different expressions of the interface force f in the framework of the reduced relaxed micromorphic simulation, which are a reasonable interpolation of this Cauchy traction, until the reduced relaxed micromorphic simulation achieves a good quantitative agreement in terms of displacement field (Fig. 13). The interface force needed to achieve a good quantitative agreement at 1400 Hz is shown in Fig. 12. We apply the same reasoning for a frequency of 2000 Hz and also for the example of "metamaterial interface" presented in the next section. [5] The analogous calibration of the interface force at 2000 Hz is shown in Fig. 14. The quantitative improvement brought by the introduction of such interface force at 2000 Hz is given in Fig. 15.

[3] To avoid the situation in which a displacement and a force are a applied on the same interface, we slightly modify the simulation setup defined in Fig. 9: instead of assigning the displacement $\overline{u}$ directly on the micromorphic continuum, we put a very thin ring of Cauchy material in perfect contact with the micromorphic continuum. In this way, we can apply the displacement $\overline{u}$ on one side of the Cauchy ring and the interface force as a non-vanishing jump arising at the Cauchy/reduced relaxed micromorphic interface, see Fig. 10. Clearly, we checked that the introduction of the Cauchy bar introduces only negligible changes to the solution when considering $[\![t]\!] = 0$.

[4] The Cauchy traction which is here inspected is the one arising at the boundary where the load is applied. Indeed, in the α-cut microstructured simulation, the considered interface is fully solid, so that the traction field can be plotted along the whole surface of interest, see Fig. 8 *(left)*. Given that the microstructured simulation is implemented using classical elasticity, the traction arising at the α-boundary is a Cauchy-like traction. The plot of the Cauchy traction field along the surface where the displacement is applied, is given in Fig. 12 and Fig. 14.

[5] The choice of the interface forces needed to reproduce the correct macro-displacement field at the targeted frequencies was achieved via a simple comparison of (i) the macroscopic interface force with the corresponding force in the microstructured simulation, and (ii) the effect of the macroscopic interface force on the solution for the displacement field. Further works could be devoted to systematic optimization procedures, once the main features of these macroscopic forces are integrally unveiled.

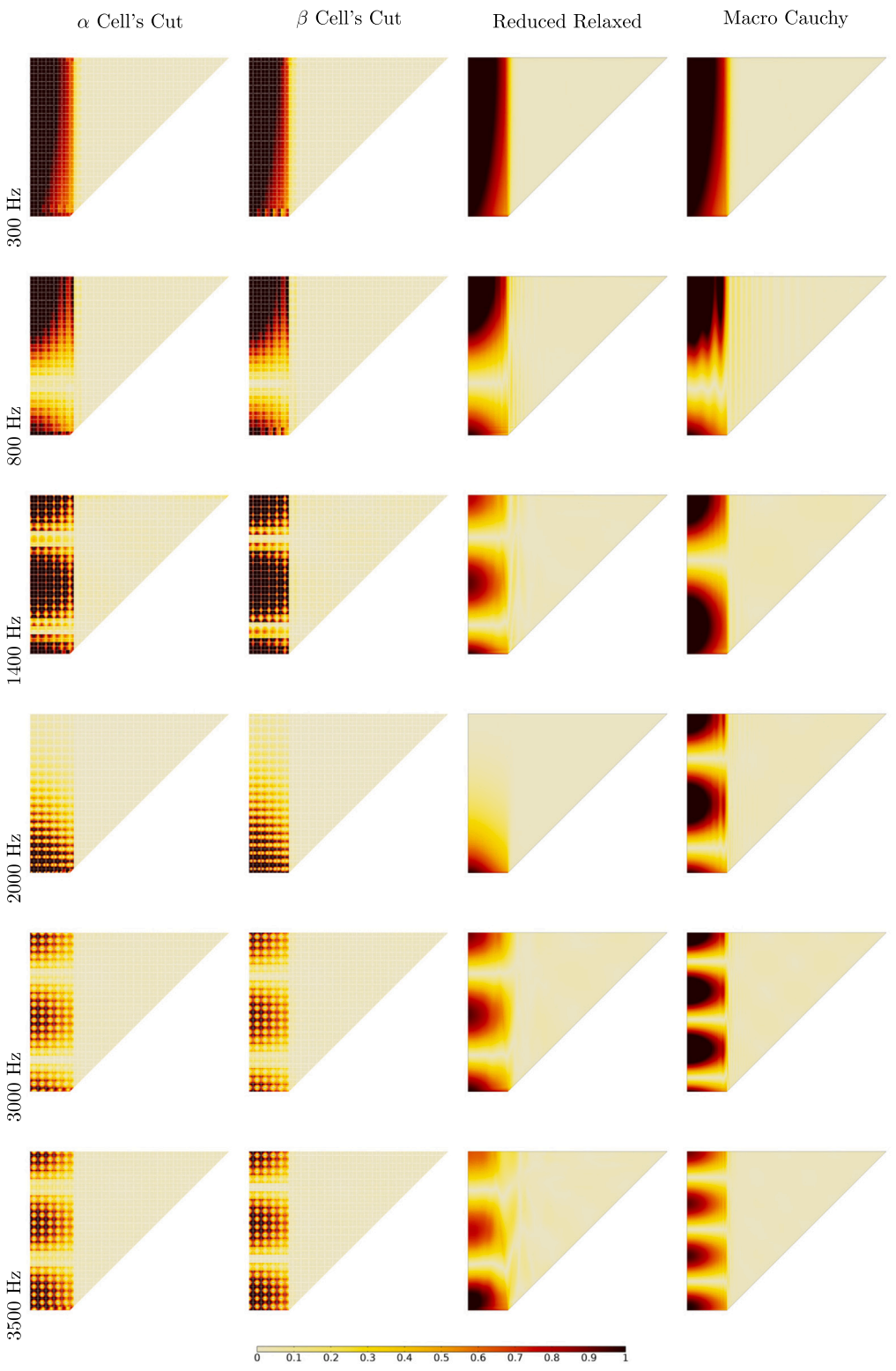

Fig. 11. Results of free interface domain simulations for different frequencies. *(First column)* α unit cell's cut microstructured simulations, *(second column)* β unit cell's cuts for different microstructured simulations, *(third column)* reduced relaxed micromorphic simulations with $f_{\text{interface}} = 0$, *(fourth column)* tetragonal Cauchy simulations with $f_{\text{interface}} = 0$.

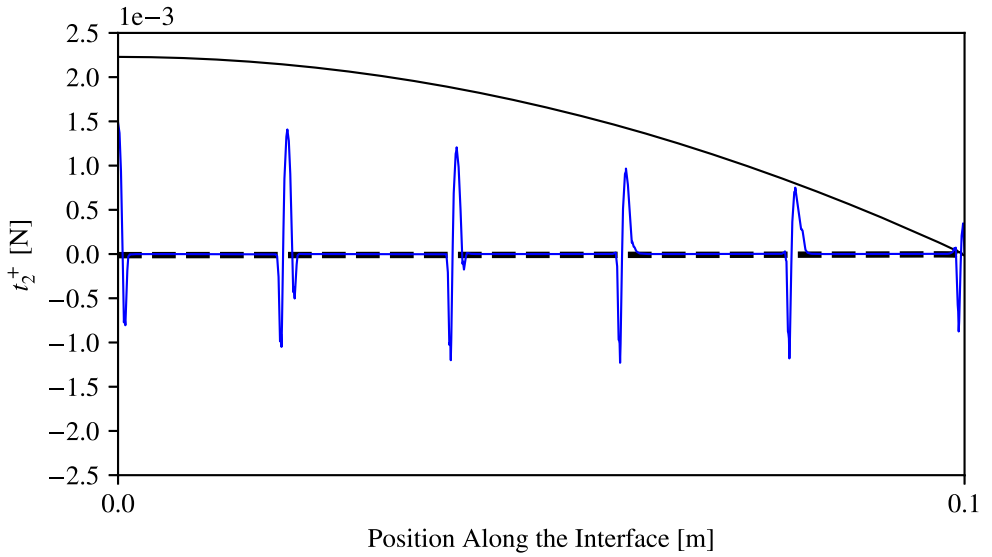

Fig. 12. Plot of the traction at $\omega = 1400$ Hz on the Cauchy side of the metamaterial interface as obtained from *(blue line)* the microstructured simulation, *(dashed line)* the reduced relaxed micromorphic simulation with no interface force, and *(black line)* the reduced relaxed micromorphic simulation with the interface force $f_1 = 0,\ f_2 = 2.25\times10^{-3}\,\frac{0.1^2 - x^2}{0.1^2},\ f_3 = 0$.

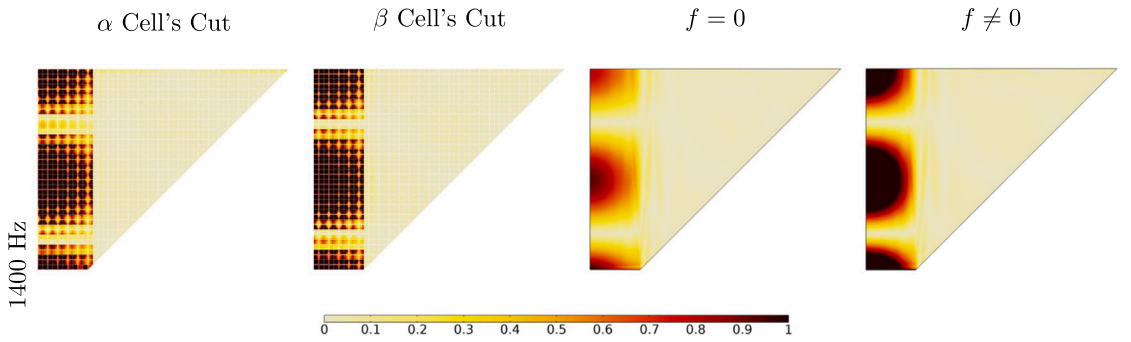

Fig. 13. Comparison at $\omega = 1400$ Hz of free interface *(first column)* α unit cell's cut microstructured simulation, *(second column)* β unit cell's cut microstructured simulation, *(third column)* coherent reduced relaxed micromorphic simulation with $f = 0$, and *(fourth column)* non-coherent reduced relaxed micromorphic simulation with $f_1 = 0,\ f_2 = 2.25\times10^{-3}\,\frac{0.1^2 - x^2}{0.1^2},\ f_3 = 0$. Here, f_i are the components of f of Eq. (13).

Summarizing the main findings of this section, we can say that the "free interface" problem defined in Fig. 7 is such that:

- The macroscopic responses associated to the α and β unit cell's cuts are very similar. The only small differences, if any, appear close to the interface where the external load is applied (see *first* and *second column* in Fig. 11).
- The reduced relaxed micromorphic model, with classical free interface conditions (7), provides a good qualitative agreement with the microstructured response (*third column* in Fig. 11). However, quantitative deviations can be detected, especially close to the band-gap region. These quantitative deviations are corrected when considering suitable interface forces arising close to the loading interface (see Figs. 13 and 15).
- The main quantitative deviations of the reduced relaxed micromorphic model with no interface force are found for frequencies close and belonging to the band-gap: this is associated to the fact that local resonances concentrated close to the boundary can trigger microstructure-related interface forces.
- A quadratic interface force applied in the vicinity of the externally loaded interface was successful in adjusting the quantitative deviations occurring for frequencies, close and belonging to the band-gap region. The intensity of the needed interface force seems to increase with frequency.
- The intensity and shape of the reduced relaxed micromorphic interface force were calibrated using the microstructured traction at the same interface as a reference case.

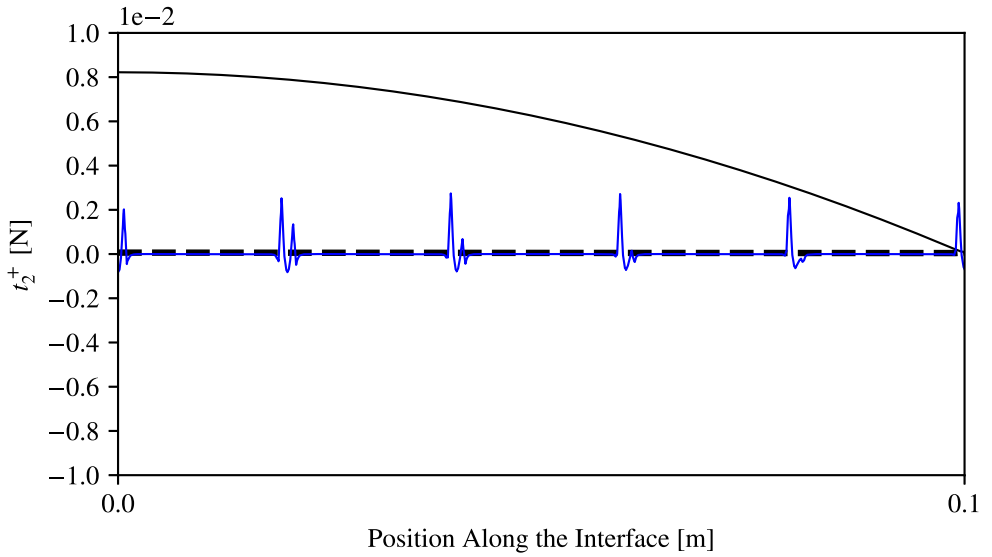

Fig. 14. Plot of the traction at $\omega = 2000$ Hz on the Cauchy side of the metamaterial interface as obtained from *(blue line)* the microstructured simulation, *(dashed line)* the reduced relaxed micromorphic simulation with no interface force, and *(black line)* the reduced relaxed micromorphic simulation with the interface force $f_1 = 0,\ f_2 = 8\times10^{-3}\,\frac{0.1^2 - x^2}{0.1^2},\ f_3 = 0$.

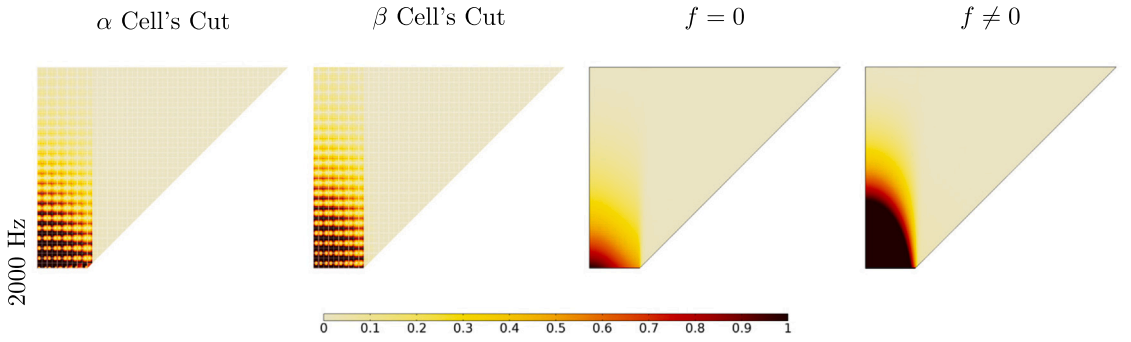

Fig. 15. Comparison at $\omega = 2000$ Hz of free interface *(first column)* α unit cell's cut microstructured simulation, *(second column)* β unit cell's cut microstructured simulation, *(third column)* coherent reduced relaxed micromorphic simulation with $f = 0$, and *(fourth column)* non-coherent reduced relaxed micromorphic simulation with $f_1 = 0,\ f_2 = 8\times10^{-3}\,\frac{0.1^2 - x^2}{0.1^2},\ f_3 = 0$. Here, f_i are the components of f of Eq. (13).

5. Effect of different cell's cuts on a homogeneous-material/metamaterial interface problem

In this section, we present a generalization of the problem presented in Section 4, where the finite-size metamaterial's block shown in Fig. 7 is connected to a homogeneous isotropic material with material parameters λ_{macro}, μ_{macro} and ρ_{macro} given in Table 2. Analogous simulations could be run by considering the outer material to be titanium, or any other homogeneous material. Also in this case, we implement symmetry conditions to reduce computational time (see Appendix A.1).

Similarly to what is done in Section 4, the metamaterial domain of Fig. 16 is modeled using titanium as the base material of the unit cell, (see Table 1), whose response is described by classical isotropic linear elasticity. A perfect connection is supposed to take place at the metamaterial/homogeneous material contact regions, which implies continuity of displacement and of tractions at the solid/solid contacts (green lines in Figs. 16 and 17). It is worth to remark that structures of the type presented in Fig. 16 are easily manufactured via metal etching techniques (Demore et al., 2022), or also via 3D printing when choosing a polymer as base material. The reduced relaxed micromorphic problem corresponding to the one defined in Fig. 16 is shown in Fig. 18. The exterior boundary of the Cauchy medium is left unconstrained in both the microstructured and the reduced relaxed micromorphic simulations.

Fig. 19 shows the solution for the microstructured problem defined in Fig. 16 for both the α (*first column*) and the β (*second column*) cell's cut for different frequencies. The (*third column*) of Fig. 19 shows the particular case of the reduced relaxed

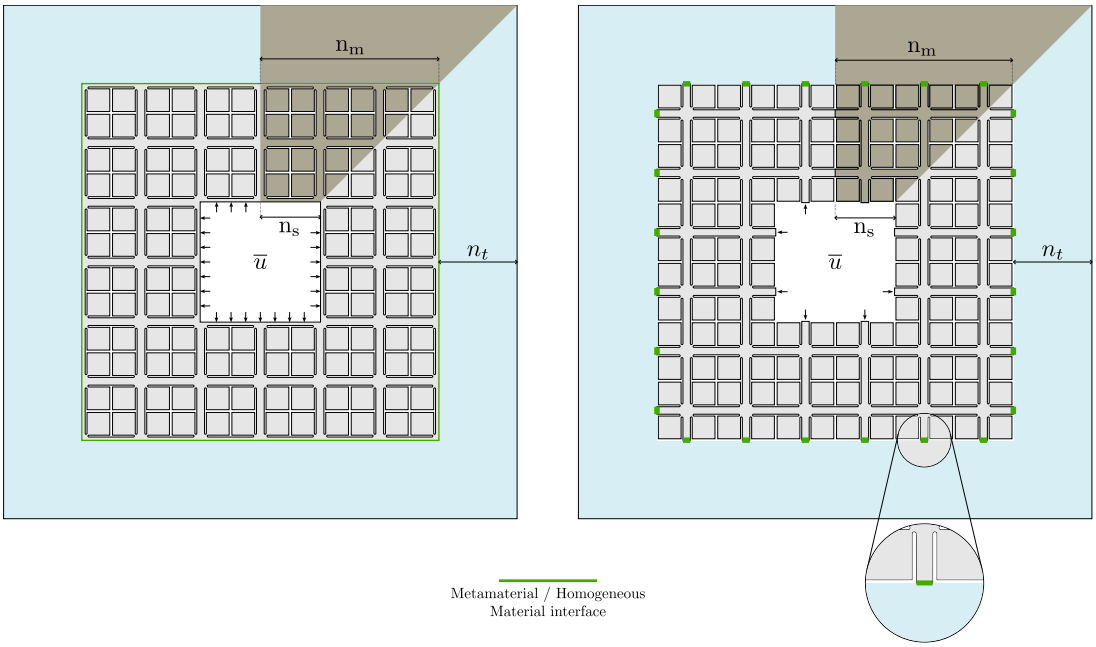

Fig. 16. Full-microstructure setup of the metamaterial/homogeneous material problem for the *(left)* α and *(right)* β unit cell's cut.

Fig. 17. Symmetrized domain for the metamaterial/homogeneous material interface problem with *(left)* α and *(right)* β unit cell's cut.

micromorphic problem of Fig. 18, obtained when setting $[\![t]\!] = 0$. The (*fourth column*) shows a reference solution where the metamaterial region is replaced by a Cauchy continuum with tetragonal symmetry, which is the long-wave limit of our micromorphic continuum (see Table 2 for its elastic coefficients).

By direct inspection of Fig. 19, we can remark that, contrarily to what happens in the "free interface" case (see Fig. 11), the difference between the α and β cell's cut is drastic, especially for frequencies below the band-gap region. This means that the simple change of the interface conditions due to the different $\alpha-$ and $\beta-$type connections to the homogeneous material is responsible for a major change in the bulk solution both in the metamaterial and in the homogeneous material region. Concerning the reduced relaxed micromorphic implementation with $[\![t]\!] = 0$ (*third column*), we can see that it gives results very similar to the unit cell's cut

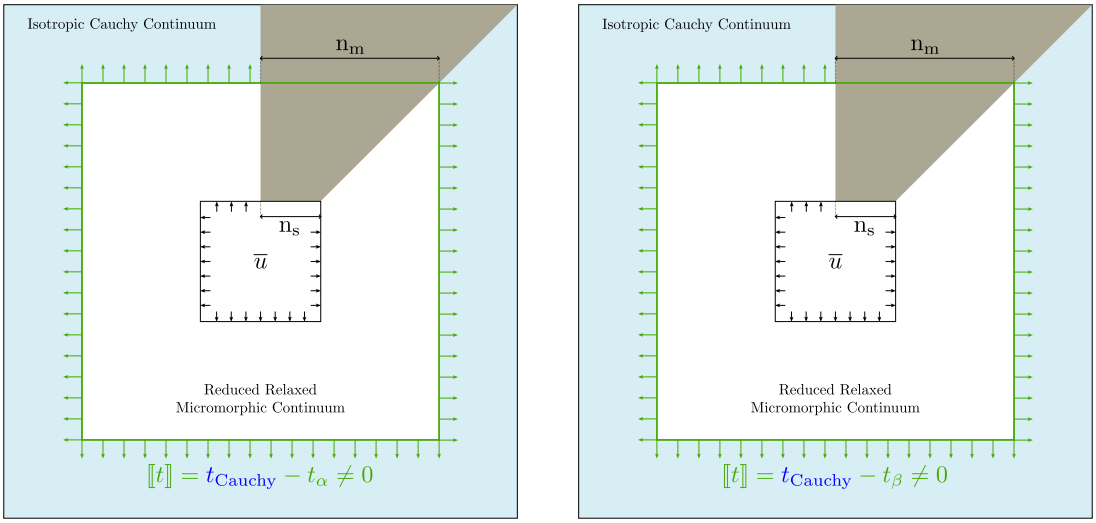

Fig. 18. Reduced relaxed micromorphic formulation of the problem shown in Fig. 16. The displacement at the metamaterial's interface is continuous, while the traction is discontinuous and depends on the type of considered unit cell's cut.

α and is thus rather different from the β cell solution. The Cauchy long-wave limit solution with $[\![t]\!] = 0$ is also similar to the α cut solution, even if it starts deviating at relatively low frequencies where only the reduced relaxed micromorphic model remains accurate. The fact that the particular reduced relaxed micromorphic solution with $[\![t]\!] = 0$ is very close to the α-type interface is indeed reasonable, since the unit cell's cut α provides a full solid interface in contact with the homogeneous material, which is a situation no too distant from the case of two homogeneous materials in perfect contact (for which the condition $[\![t]\!] = 0$ is known to be the correct one). On the other hand, the unit cell's cut β provides an almost empty interface across which the solid connections are given by thin bars. It is thus sensible to hypothesize that an interface traction jump $[\![t]\!] \neq 0$ is activated close to the β interface. To prove this, we show in Figs. 22–31 the change of solution which is provided when activating a traction jump $[\![t]\!] \neq 0$. It can be inferred that when suitably tuning the value of $[\![t]\!]$, the $\beta-$cell solution can be recovered. The difference between the $\alpha-$ and $\beta-$cut solutions becomes smaller for frequencies starting around the band-gap region and higher, even if such difference is still present (see Fig. 19). For frequencies close and belonging to the band-gap region, a small correction to the interface force close to the application of the external load, can be given in the reduced relaxed micromorphic case to improve the slight quantitative difference with respect to the microstructured solution, as already done in the "free interface" problem in Section 4.

In order to bring the reduced relaxed micromorphic solution close to the β-cut microstructured one, we must look for a suitable form of the interface force triggered at the reduced relaxed micromorphic/homogeneous material interface. To do so, we proceed similarly to what is done in Section 4 for the "free interface" case and perform a calibration of the interface force $f^{interface}$ for each frequency. In particular, we start comparing the traction on the Cauchy side of the interface as arising from the full-microstructured β-type simulation and the equivalent traction arising from the reduced relaxed micromorphic simulation when setting $[\![t]\!] = 0$. For clarity of exposition, we will denote $t^+_{\beta-\text{Microstructure}}$ and t^+_{Cauchy} the traction arising on the Cauchy side of the interface in the microstructured and reduced relaxed micromorphic simulations, respectively (see Fig. 20)

The calibration procedure for the interface force at $\omega = 250$ Hz is shown in Fig. 21. As mentioned above, we start by inspecting the behavior of the Cauchy traction of the reduced relaxed micromorphic simulation with $[\![t]\!] = 0$ *(dashed lined)* and comparing it with the trend of the Cauchy traction issued from the full-microstructured simulation. We then make an ansatz on the interface force to be such that $f^{\text{interface}} = \alpha t_{\text{micromorphic}}$ and we see which is the effect of varying the α parameter on the Cauchy traction. This simplified ansatz on the form of $f^{\text{interface}}$ was sufficient to retrieve the correct solution for some frequencies. For other frequencies the ansatz on $f^{\text{interface}}$ had to be more complex and it is indicated in the captions of the corresponding figures (see Figs. 23–31). For the frequency $\omega = 2850$ Hz, an interface force was needed to adjust both the α and β cuts: this might be due to the fact that for higher frequencies the wavelength becomes comparable to the cell's size. Two different calibration procedures were thus needed as shown in Figs. 29 and 30.

As shown for the "free interface" case, small quantitative deviations of the reduced relaxed micromorphic solutions from the microstructured ones can be found for frequencies close or inside the band-gap (see e.g. $\omega = 2000$ Hz in Fig. 19). As shown before for the "free interface case", those small deviations can be easily adjusted considering a quadratic interface force close to the application of the external load. Since the results are analogous to the ones presented before, we do not present specific pictures here and we refer to Fig. 15 for possible reference.

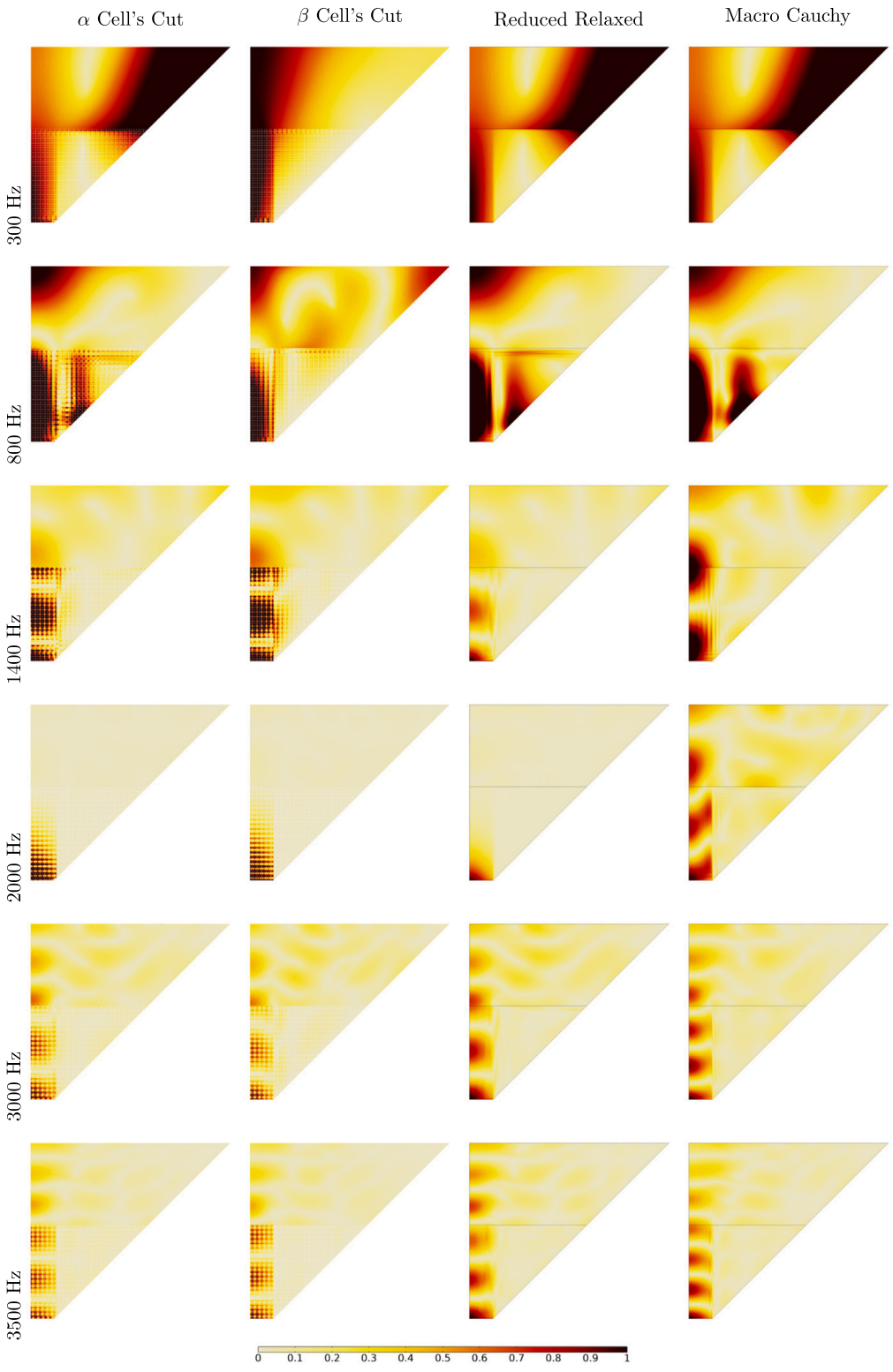

Fig. 19. Results of free interface domain simulations for different frequencies. *(First column)* α unit cell's cut microstructured simulations, *(second column)* β unit cell's cuts for different microstructured simulations, *(third column)* reduced relaxed micromorphic simulations with $[\![t]\!] = 0$, *(fourth column)* tetragonal Cauchy simulations with $[\![t]\!] = 0$.

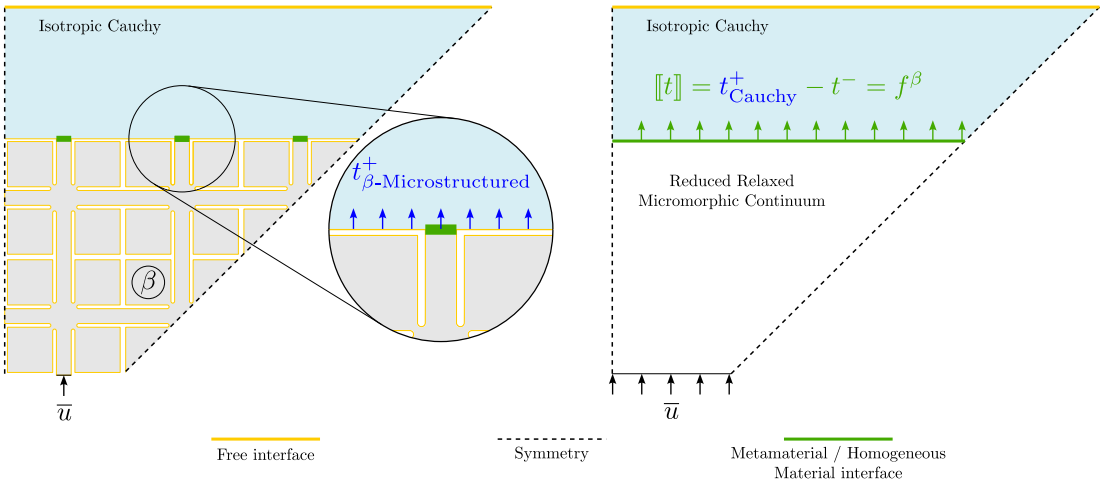

Fig. 20. *(Left)* Representation of the traction $t^+_{\beta-\text{Microstructure}}$ arising on the Cauchy side of the microstructured simulation: since the Cauchy material is homogeneous, the interface reported from the Cauchy side is continuous, thus allowing the line-plot of the traction along the interface. *(Right)* Representation of the interface force $f^\beta := t^+_{\text{Cauchy}} - t^-_{\beta-\text{Microstructure}}$ at the reduced relaxed micromorphic/Cauchy interface: in order to compare analogous quantities, only $t^+_{\beta-\text{Microstructure}}$ and t^+_{Cauchy} will be compared in the following plots.

The analysis of Figs. 21–31 brings us to important conclusions, significantly advancing the state of the art concerning the macroscopic modeling of mechanical metamaterials. We summarize the main findings as follows:

- The metamaterial interface which is connected to the homogeneous material through a full-solid connection (α unit cell type) is well described by the reduced relaxed micromorphic model with interface conditions $[\![u]\!] = 0$ and $[\![t]\!] = 0$.
- The metamaterial interface which is connected to the homogeneous material with thin bars and empty-space elsewhere (β unit cell type) can no longer be described by the boundary conditions $[\![u]\!] = 0$ and $[\![t]\!] = 0$, when considering the reduced relaxed micromorphic formulation of the problem. In this case, the macroscopic reduced relaxed micromorphic/Cauchy interface must be considered to be an elastic interface: $[\![u]\!] = 0$ and $[\![t]\!] \neq 0$.
- The difference between the $\alpha-$ and $\beta-$type solutions is more pronounced in the frequency region which goes from approximately 2000 Hz to the lower band-gap limit (approx. 1700 Hz). Given that such differences were not present in the "free interface" problem (Fig. 11), this is most likely due to the fact that the wavelengths in this frequency range have a characteristic size comparable with the length of the metamaterial/homogeneous material interface (1 m), while for frequencies higher than 2000 Hz the wavelengths become small with respect to the interface. This suggests that the considered interface indeed acts as an "obstacle" for the traveling waves which behaves differently in the α and β case. In other words, we can say that, for the considered frequencies, such a macroscopic interface can be seen as a "material interface" with its own elastic properties that are conferred to the interface itself from the characteristics of the underlying microstructure.
- For very low frequencies (up to 300–400 Hz), the metamaterial response can be caught rather well by a macroscopic Cauchy model with tetragonal symmetry. This means that at low frequencies the anisotropy alone is sufficient to account for the macroscopic heterogeneity driven by the underlying microstructure. Using "classical" interface conditions or "elastic interface" conditions allows to discriminate between the α and the β solution also in the simplified case of Cauchy elasticity, when the frequency remains small enough to avoid the activation of dispersive phenomena.
- For frequencies higher than 400 Hz, dispersive phenomena start taking place due to a more complex interaction of the wave with the underlying microstructure, so that a reduced relaxed micromorphic model is necessary to catch this complex response. As said before, the reduced relaxed micromorphic model can discriminate between the α and β solutions by switching from the condition $[\![t]\!] = 0$ to the condition $[\![t]\!] \neq 0$.
- Considering adequate interface forces at the reduced relaxed micromorphic/homogeneous material interface can account for the large differences in the solution between the α and β cut for frequencies lower than the band-gap.
- Small quantitative deviations of the reduced relaxed micromorphic solutions from the microstructured solution close and inside the band-gap region, can once again be re-adjusted by considering the presence of an interface force close to the application of the external load.

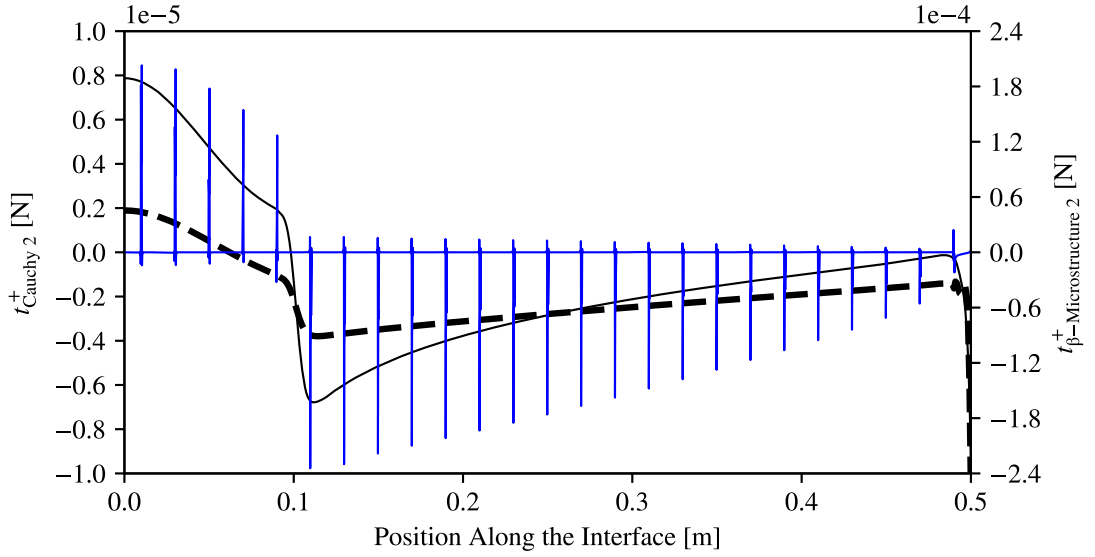

Fig. 21. Plot of the traction at $\omega = 250$ Hz on the Cauchy side of the metamaterial interface as obtained from *(blue line)* the microstructured simulation, *(dashed line)* the reduced relaxed micromorphic simulation with no interface force, and *(black line)* the reduced relaxed micromorphic simulation with the interface force $f^\beta_1 = 0,\ f^\beta_2 = -2.2\, t^-_2,\ f^\beta_3 = 0$.

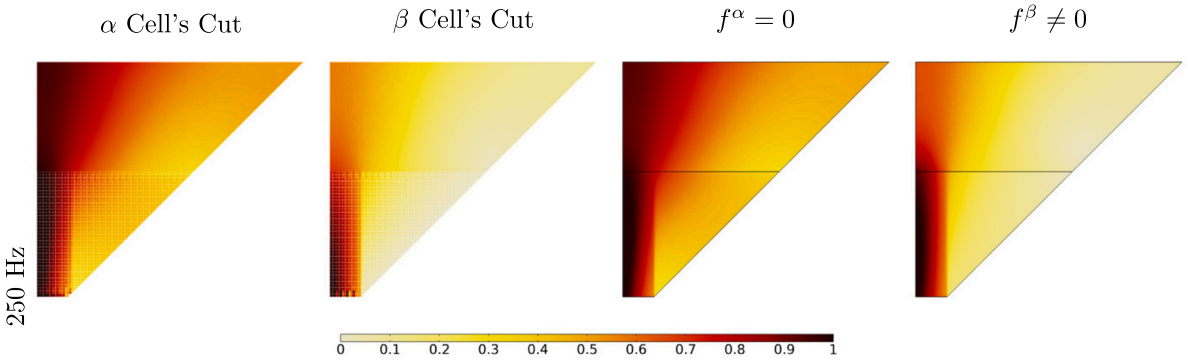

Fig. 22. Comparison at $\omega = 250$ Hz of solid/metamaterial interface *(first column)* α unit cell's cut microstructured simulation, *(second column)* β unit cell's cut microstructured simulation, *(third column)* coherent reduced relaxed micromorphic simulation with $[\![t]\!] = f = f^\alpha = 0$, and *(fourth column)* non-coherent reduced relaxed micromorphic simulation with $[\![t]\!] = f = f^\beta \neq 0$ and $f^\beta_1 = 0,\ f^\beta_2 = -2.2\, t^-_2,\ f^\beta_3 = 0$. Here, t^-_i and f_i are the components of the micromorphic traction t^- and of the force f of Eq. (13).

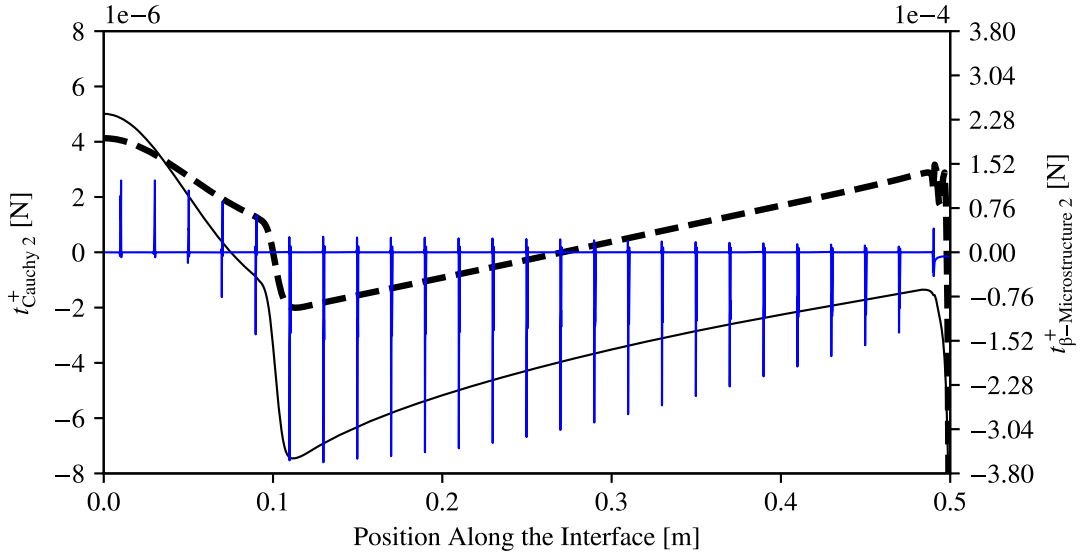

Fig. 23. Plot of the traction at $\omega = 300$ Hz on the Cauchy side of the metamaterial interface as obtained from *(blue line)* the microstructured simulation, *(dashed line)* the reduced relaxed micromorphic simulation with no interface force, and *(black line)* the reduced relaxed micromorphic simulation with the interface force $f^\beta_1 = 0,\ f^\beta_2 = -1.6\, t^-_2,\ f^\beta_3 = 0$.

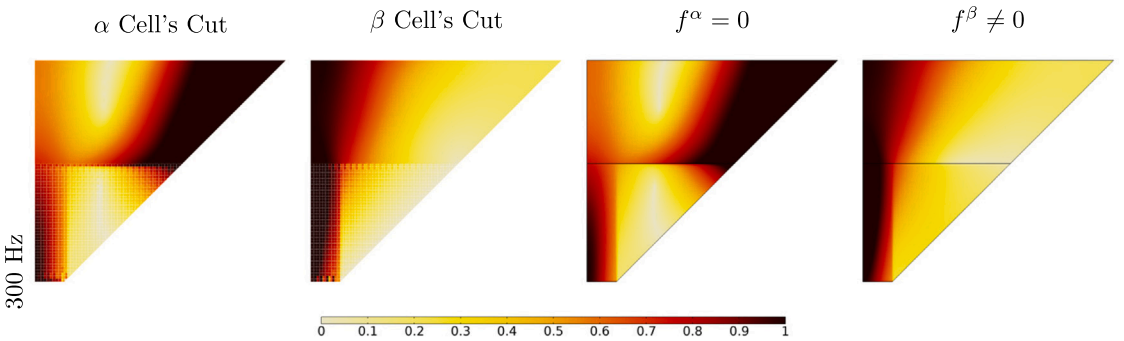

Fig. 24. Comparison at $\omega = 300$ Hz of solid/metamaterial interface *(first column)* α unit cell's cut microstructured simulation, *(second column)* β unit cell's cut microstructured simulation, *(third column)* coherent reduced relaxed micromorphic simulation with $[\![t]\!] = f = f^\alpha = 0$, and *(fourth column)* non-coherent reduced relaxed micromorphic simulation with $[\![t]\!] = f = f^\beta \neq 0$ and $f^\beta_1 = 0,\ f^\beta_2 = -1.6\, t^-_2,\ f^\beta_3 = 0$. Here, t^-_i and f_i are the components of the micromorphic traction t^- and of the force f of Eq. (13).

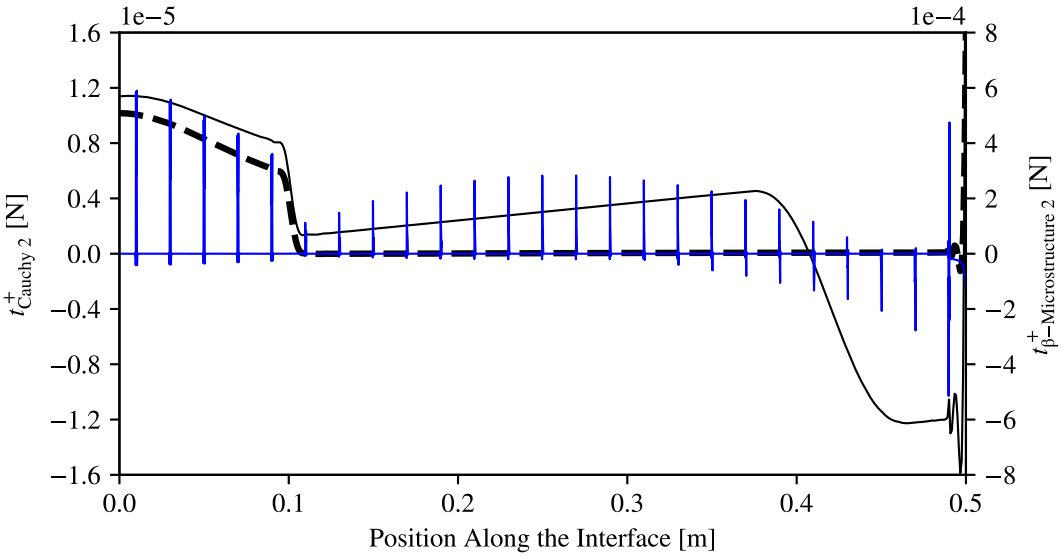

Fig. 25. Plot of the traction at $\omega = 450$ Hz on the Cauchy side of the metamaterial interface as obtained from *(blue line)* the microstructured simulation, *(dashed line)* the reduced relaxed micromorphic simulation with no interface force, and *(black line)* the reduced relaxed micromorphic simulation with the interface force $f^\beta_1 = 0,\ f^\beta_2 = \frac{6\times10^{-6}}{0.5}x - 1.8\times10^{-5}\mathrm{H}(x-0.42),\ f^\beta_3 = 0.$

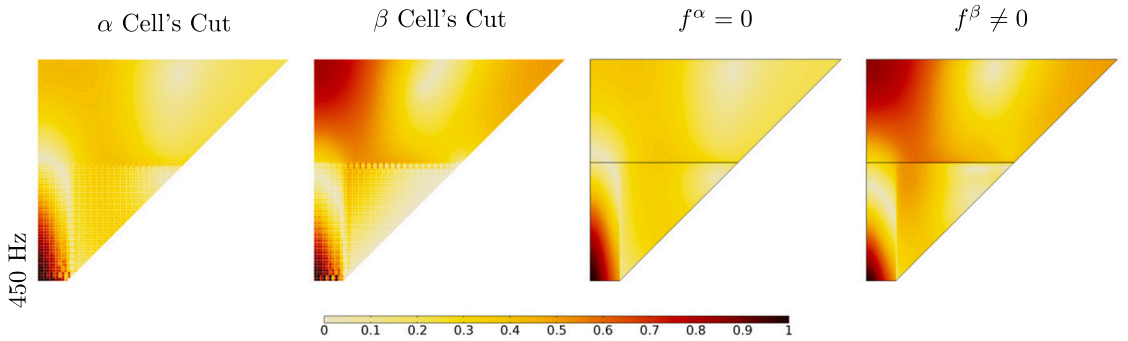

Fig. 26. Comparison at $\omega = 450$ Hz of solid/metamaterial interface *(first column)* α unit cell's cut microstructured simulation, *(second column)* β unit cell's cut microstructured simulation, *(third column)* coherent reduced relaxed micromorphic simulation with $[\![t]\!] = f = f^\alpha = 0$, and *(fourth column)* non-coherent reduced relaxed micromorphic simulation with $[\![t]\!] = f = f^\beta \neq 0$ and $f^\beta_1 = 0,\ f^\beta_2 = \frac{6\times10^{-6}}{0.5}x - 1.8\times10^{-5}\mathrm{H}(x-0.42),\ f^\beta_3 = 0$. Here, f_i are the components of the force f of Eq. (13), and H is the Heaviside step function with a transition zone of 0.1 m.

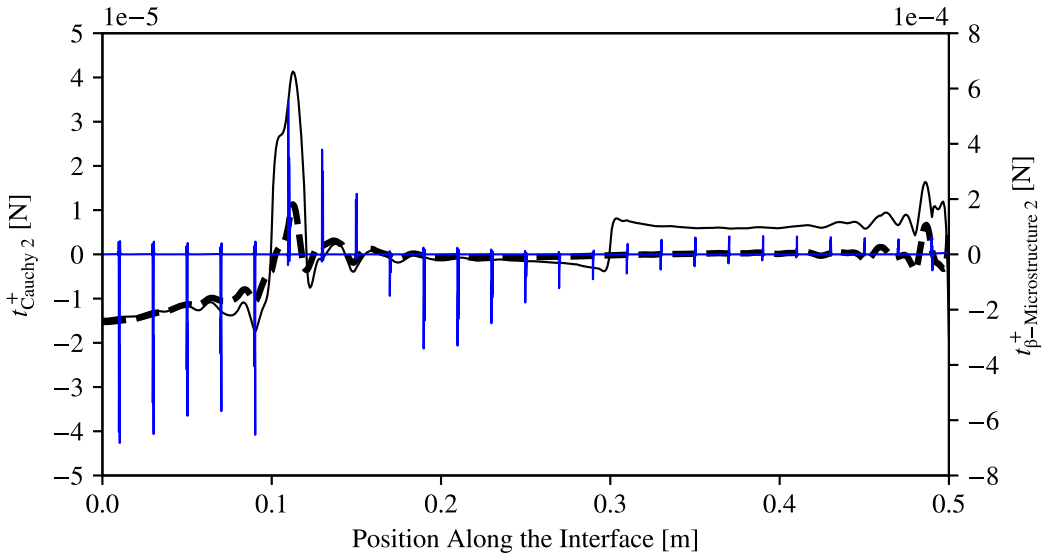

Fig. 27. Plot of the traction at $\omega = 1050$ Hz on the Cauchy side of the metamaterial interface as obtained from *(blue line)* the microstructured simulation, *(dashed line)* the reduced relaxed micromorphic simulation with no interface force, and *(black line)* the reduced relaxed micromorphic simulation with the interface force $f^\beta_1 = 0$, $f^\beta_2 = 3\times10^{-6}\mathrm{H}(0.1 - x) + 3\times10^{-5}(\mathrm{H}(x - 0.1) - \mathrm{H}(0.12 - x)) + 1.2\times10^{-5}\mathrm{H}(x - 0.3)$, $f^\beta_3 = 0$.

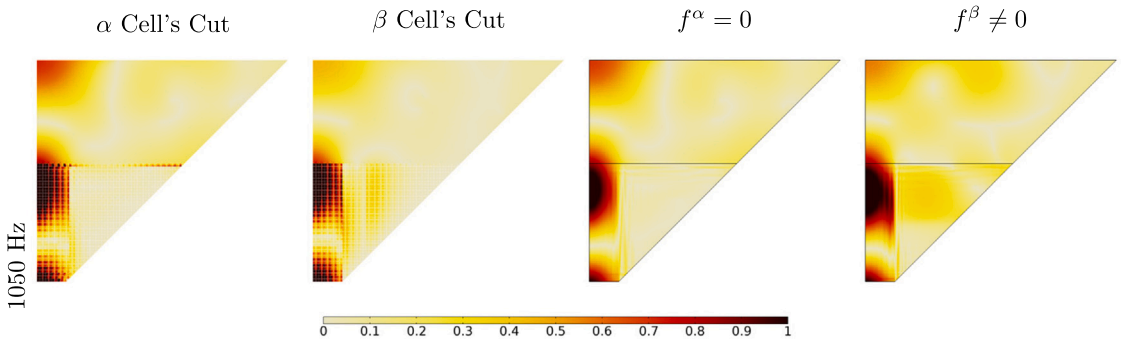

Fig. 28. Comparison at $\omega = 1050$ Hz of solid/metamaterial interface *(first column)* α unit cell's cut microstructured simulation, *(second column)* β unit cell's cut microstructured simulation, *(third column)* coherent reduced relaxed micromorphic simulation with $[\![t]\!] = f = f^\alpha = 0$, and *(fourth column)* non-coherent reduced relaxed micromorphic simulation with $[\![t]\!] = f = f^\beta \neq 0$ and $f^\beta_1 = 0$, $f^\beta_2 = 3\times10^{-6}\mathrm{H}(0.1 - x) + 3\times10^{-5}(\mathrm{H}(x - 0.1) - \mathrm{H}(0.12 - x)) + 1.2\times10^{-5}\mathrm{H}(x - 0.3)$, $f^\beta_3 = 0$. Here, f_i are the components of the force f of Eq. (13), and H is the Heaviside step function with a transition zone of 0.005 m.

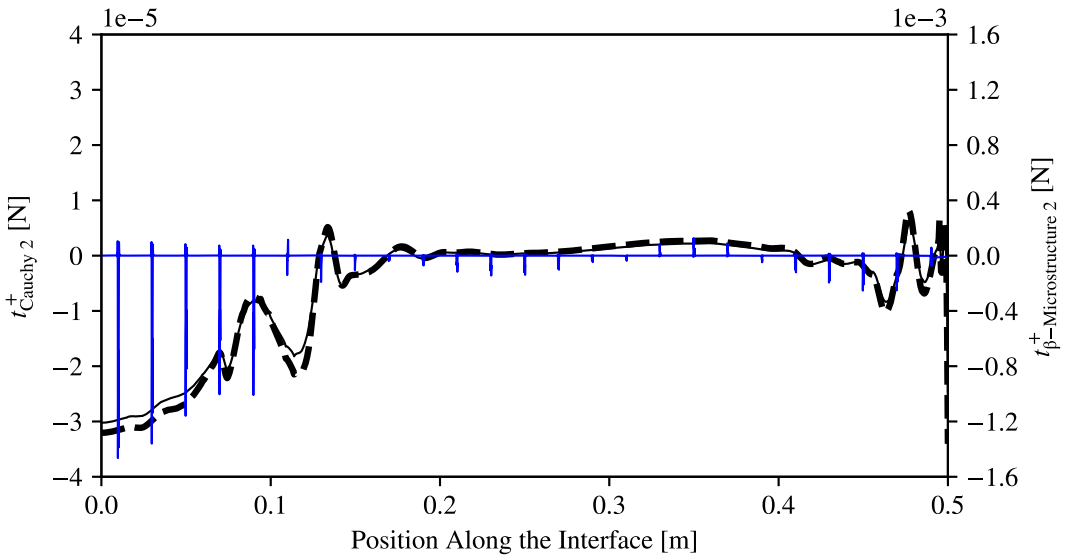

Fig. 29. Plot of the traction at ω = 2850 Hz on the Cauchy side of the β unit cell metamaterial interface as obtained from *(blue line)* the microstructured simulation, *(dashed line)* the reduced relaxed micromorphic simulation with no interface force, and *(black line)* the reduced relaxed micromorphic simulation with the interface force $f_1^\beta = 0$, $f_2^\beta = 0.2\, t_2^-$, $f_3^\beta = 0$.

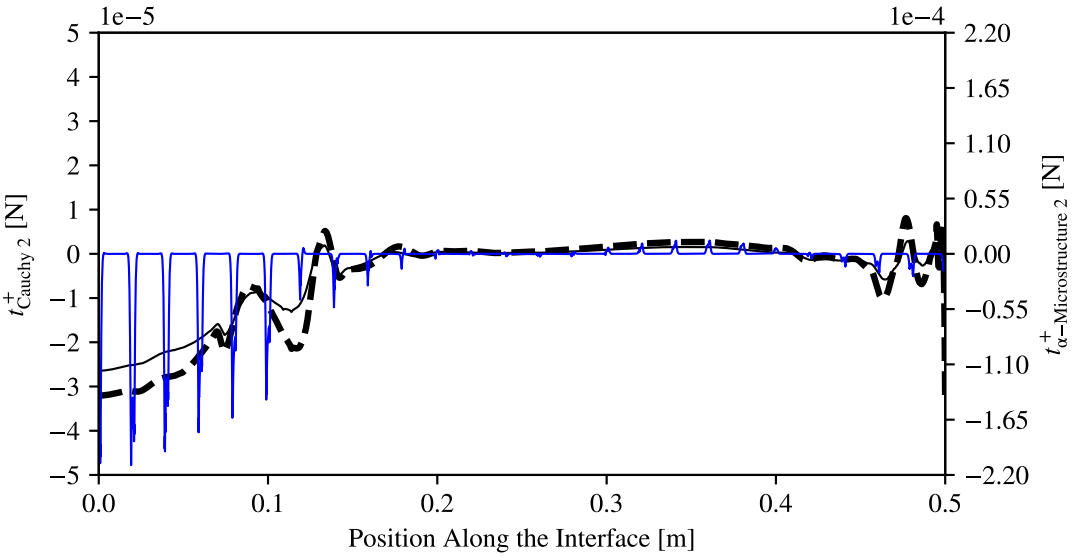

Fig. 30. Plot of the traction at ω = 2850 Hz on the Cauchy side of the α unit cell metamaterial interface as obtained from *(blue line)* the microstructured simulation, *(dashed line)* the reduced relaxed micromorphic simulation with no interface force, and *(black line)* the reduced relaxed micromorphic simulation with the interface force $f_1^\alpha = 0$, $f_2^\alpha = 0.45\, t_2^-$, $f_3^\alpha = 0$.

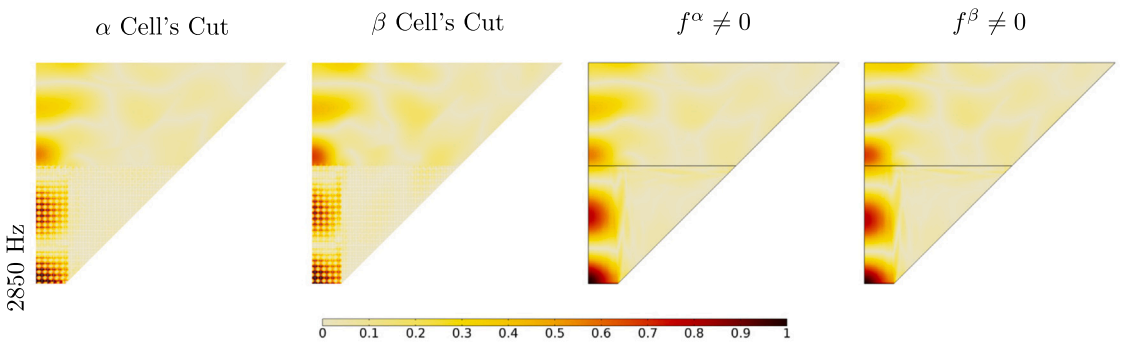

Fig. 31. Comparison at $\omega = 2850$ Hz of solid/metamaterial interface *(first column)* α unit cell's cut microstructured simulation, *(second column)* β unit cell's cut microstructured simulation, *(third column)* non-coherent reduced relaxed micromorphic simulation with $[\![t]\!] = f = f^\alpha \neq 0$ and $f_1^\alpha = 0$, $f_2^\alpha = 0.45\, t_2^-$, $f_3^\alpha = 0$, and *(fourth column)* non-coherent reduced relaxed micromorphic simulation with $[\![t]\!] = f = f^\beta \neq 0$ and $f_1^\beta = 0$, $f_2^\beta = 0.2\, t_2^-$, $f_3^\beta = 0$. Here, t_i^- and f_i are the components of the micromorphic traction t^- and of the force f of Eq. (13).

6. Conclusions and perspective

In this paper, we showed for the first time that the modeling of mechanical metamaterials at the homogenized scale necessarily requires the introduction of the concept of "non-coherent" interfaces when considering metamaterial specimens of finite-size. In particular, we proved that the introduction of interface forces which are able to discriminate between two different unit cell's cuts, is of paramount importance if one wants to use macroscopic (homogenized) models to describe the response of metamaterial's blocks of finite-size. The need of introducing such interface forces has been clearly explained through the presentation of two different examples in which interface forces are defined in the context of reduced relaxed micromorphic elasticity. The results presented in this paper are a fundamental milestone for the understanding of the way in which metamaterials should be modeled when considering finite-size blocks at the engineering scale. Given the novelty of the obtained results, the present paper opens new perspectives for further studies which will be oriented to understand the effect on interface forces of:

- the macroscopic geometry of the bulk domains and of the interfaces and intensity,
- the type and intensity of the applied load,
- the size of the metamaterial's specimen, and
- the considered frequency.

CRediT authorship contribution statement

Leonardo A. Perez Ramirez: Writing – review & editing, Writing – original draft, Visualization, Validation, Software, Methodology, Investigation, Formal analysis. **Félix Erel-Demore:** Software. **Gianluca Rizzi:** Software. **Jendrik Voss:** Software. **Angela Madeo:** Writing – review & editing, Writing – original draft, Supervision, Resources, Project administration, Methodology, Investigation, Funding acquisition, Formal analysis, Conceptualization.

Declaration of competing interest

The authors declare the following financial interests/personal relationships which may be considered as potential competing interests: Angela Madeo reports financial support was provided by European Research Council. If there are other authors, they declare that they have no known competing financial interests or personal relationships that could have appeared to influence the work reported in this paper.

Data availability

The commercial code COMSOL was used for the implementation and all details are explicitly given in the paper for easily reproducing the results.

Acknowledgments

Angela Madeo, Leonardo A. Perez Ramirez, Félix Erel-Demore, and Gianluca Rizzi acknowledge support from the European Commission through the funding of the ERC Consolidator Grant META-LEGO, N° 101001759.

Annexes

A.1. Symmetry conditions of the reduced relaxed micromorphic continuum

We follow the approach of Demore et al. (2022) to define the symmetry conditions of the reduced relaxed micromorphic continuum. Let us apply Curie's Symmetry Principle (Curie, 1894) on $u \in \mathbb{R}^3$ the macroscopic displacement field and on $P \in \mathbb{R}^{3\times3}$ the non-symmetric micro-distortion field, with respect to a symmetry plane $\mathcal{N}$ of normal n:

$$\begin{cases} u(x^*) = u^*(x) \\ P(x^*) = P^*(x) \end{cases}, \tag{14}$$

where u^*, P^* are the symmetrics of u, P. We also define the corresponding orthonormal bases $\{t_1^*, t_2^*, n^*\}$ and $\{t_1, t_2, n\}$ using vectors tangent and normal to $\mathcal{N}$, such that

$$t_1^* = t_1\ ,\ t_2^* = t_2\ ,\ \text{and}\ n^* = -n\ . \tag{15}$$

We write the expansion of the u macroscopic displacement and P micro-distortion fields relative to their corresponding basis:

$$u = u_1 t_1 + u_2 t_2 + u_3 n\ , \tag{16}$$

$$\begin{aligned} P =& P_{11} t_1 \otimes t_1 + P_{12} t_1 \otimes t_2 + P_{13} t_1 \otimes n \\ &+ P_{21} t_2 \otimes t_1 + P_{22} t_2 \otimes t_2 + P_{23} t_2 \otimes n \\ &+ P_{31} n \otimes t_1 + P_{32} n \otimes t_2 + P_{33} n \otimes n\ , \end{aligned} \tag{17}$$

and

$$u^* = u_1 t_1^* + u_2 t_2^* + u_3 n^*\ , \tag{18}$$

$$\begin{aligned} P^* =& P_{11} t_1^* \otimes t_1^* + P_{12} t_1^* \otimes t_2^* + P_{13} t_1^* \otimes n^* \\ &+ P_{21} t_2^* \otimes t_1^* + P_{22} t_2^* \otimes t_2^* + P_{23} t_2^* \otimes n^* \\ &+ P_{31} n^* \otimes t_1^* + P_{32} n^* \otimes t_2^* + P_{33} n^* \otimes n^*\ , \end{aligned} \tag{19}$$

where the scalars u_i and P_{ij} are the unique components of u and P relative to both bases, and in both bases the same. If we use the equivalencies of Eq. (15), we can rewrite (18) and (19) like:

$$u^* = u_1 t_1 + u_2 t_2 - u_3 n\ , \tag{20}$$

$$\begin{aligned} P^* =& P_{11} t_1 \otimes t_1 + P_{12} t_1 \otimes t_2 - P_{13} t_1 \otimes n \\ &+ P_{21} t_2 \otimes t_1 + P_{22} t_2 \otimes t_2 - P_{23} t_2 \otimes n \\ &- P_{31} n \otimes t_1 - P_{32} n \otimes t_2 + P_{33} n \otimes n\ , \end{aligned} \tag{21}$$

Similarly, if we define the points x and x^* as $x = x_0 + \epsilon n$ and $x^* = x_0 + \epsilon n^*$, where $x_0 \in \mathcal{N}$ and $\epsilon \in \mathbb{R}$, we can say that $x^* = x_0 - \epsilon n$. Next, if we write the symmetry conditions (14) using the expansions of Eqs. (16),(17) and (20),(21), and group them in terms of their components, we reach:

$$\begin{cases} u_1(x_0 - \epsilon n) t_1 = u_1(x_0 + \epsilon n) t_1 \\ u_2(x_0 - \epsilon n) t_2 = u_2(x_0 + \epsilon n) t_2 \\ u_3(x_0 - \epsilon n) n = -u_3(x_0 + \epsilon n) n \end{cases}, \quad \begin{cases} P_{11}(x_0 - \epsilon n) t_1 \otimes t_1 = P_{11}(x_0 + \epsilon n) t_1 \otimes t_1 \\ P_{12}(x_0 - \epsilon n) t_1 \otimes t_2 = P_{12}(x_0 + \epsilon n) t_1 \otimes t_2 \\ P_{13}(x_0 - \epsilon n) t_1 \otimes n = -P_{13}(x_0 + \epsilon n) t_1 \otimes n \\ P_{21}(x_0 - \epsilon n) t_2 \otimes t_1 = P_{21}(x_0 + \epsilon n) t_2 \otimes t_1 \\ P_{22}(x_0 - \epsilon n) t_2 \otimes t_2 = P_{22}(x_0 + \epsilon n) t_2 \otimes t_2 \\ P_{23}(x_0 - \epsilon n) t_2 \otimes n = -P_{23}(x_0 + \epsilon n) t_2 \otimes n \\ P_{31}(x_0 - \epsilon n) n \otimes t_1 = -P_{31}(x_0 + \epsilon n) n \otimes t_1 \\ P_{32}(x_0 - \epsilon n) n \otimes t_2 = -P_{32}(x_0 + \epsilon n) n \otimes t_2 \\ P_{33}(x_0 - \epsilon n) n \otimes n = P_{33}(x_0 + \epsilon n) n \otimes n \end{cases}. \tag{22}$$

These symmetry conditions allow to find the values of u and P at any point in space with respect to the symmetry plane, if their value is known on the opposite side of the symmetry plane. In the limit of $\epsilon \to 0$, Eq. (22) becomes:

$$\begin{cases} u_1\left(x_0\right) t_1 = u_1\left(x_0\right) t_1 \\ u_2\left(x_0\right) t_2 = u_2\left(x_0\right) t_2 \\ u_3\left(x_0\right) n = -u_3\left(x_0\right) n \end{cases}, \quad \begin{cases} P_{11}\left(x_0\right) t_1 \otimes t_1 = P_{11}\left(x_0\right) t_1 \otimes t_1 \\ P_{12}\left(x_0\right) t_1 \otimes t_2 = P_{12}\left(x_0\right) t_1 \otimes t_2 \\ P_{13}\left(x_0\right) t_1 \otimes n = -P_{13}\left(x_0\right) t_1 \otimes n \\ P_{21}\left(x_0\right) t_2 \otimes t_1 = P_{21}\left(x_0\right) t_2 \otimes t_1 \\ P_{22}\left(x_0\right) t_2 \otimes t_2 = P_{22}\left(x_0\right) t_2 \otimes t_2 \\ P_{23}\left(x_0\right) t_2 \otimes n = -P_{23}\left(x_0\right) t_2 \otimes n \\ P_{31}\left(x_0\right) n \otimes t_1 = -P_{31}\left(x_0\right) n \otimes t_1 \\ P_{32}\left(x_0\right) n \otimes t_2 = -P_{32}\left(x_0\right) n \otimes t_2 \\ P_{33}\left(x_0\right) n \otimes n = P_{33}\left(x_0\right) n \otimes n \end{cases}. \tag{23}$$

We find that on the symmetry plane $\mathcal{N}$: $u_3 = P_{13} = P_{23} = P_{31} = P_{32} = 0$. Thus, the following conditions must be satisfied on $\mathcal{N}$:

$$\begin{cases} \langle u, n\rangle = 0 \\ \langle P, t_1 \otimes n\rangle = 0 \\ \langle P, t_2 \otimes n\rangle = 0 \\ \langle P, n \otimes t_1\rangle = 0 \\ \langle P, n \otimes t_2\rangle = 0 \end{cases}. \tag{24}$$

For a plane strain problem, the displacement field has $u_3 = 0$ and the microdistortion tensor has $P_{3i} = 0$. Thus, for a vertical symmetry plane: $t_1 = (0,0,1), t_2 = (0,1,0), n = (1,0,0)$, with t_1 and t_2 arbitrary tangents, the symmetry conditions (24) reduce to:

$$\begin{cases} \langle u, n\rangle = u_1 = 0 \\ \langle P, t_1 \otimes n\rangle = 0 = 0 \\ \langle P, t_2 \otimes n\rangle = P_{21} = 0 \\ \langle P, n \otimes t_1\rangle = 0 = 0 \\ \langle P, n \otimes t_2\rangle = P_{12} = 0 \end{cases}. \tag{25}$$

Equivalently, for a symmetry plane at 45°: $t_1 = (0,0,1), t_2 = (\frac{1}{\sqrt{2}}, \frac{1}{\sqrt{2}}, 0), n = (-\frac{1}{\sqrt{2}}, \frac{1}{\sqrt{2}}, 0)$, with t_1 and t_2 arbitrary tangents, the symmetry conditions (24) reduce to:

$$\begin{cases} \langle u, n\rangle = -u_1 + u_2 = 0 \\ \langle P, t_1 \otimes n\rangle = 0 = 0 \\ \langle P, t_2 \otimes n\rangle = -P_{11} + P_{12} - P_{21} + P_{22} = 0 \\ \langle P, n \otimes t_1\rangle = 0 = 0 \\ \langle P, n \otimes t_2\rangle = -P_{11} - P_{12} + P_{21} + P_{22} = 0 \end{cases}. \tag{26}$$

References

Adam, N.K., 1941. The Physics and Chemistry of Surfaces, third edition Oxford University Press, London.

Adamson, A.W., Gast, A.P., 1967. Physical Chemistry of Surfaces. Interscience, New York-London.

Aivaliotis, A., Tallarico, D., d'Agostino, M.-V., Daouadji, A., Neff, P., Madeo, A., 2020. Frequency- and angle-dependent scattering of a finite-sized meta-structure via the relaxed micromorphic model. Arch. Appl. Mech. 90 (5), 1073–1096.

Alfano, G., Crisfield, M.A., 2001. Finite element interface models for the delamination analysis of laminated composites: Mechanical and computational issues. Internat. J. Numer. Methods Engrg. 50 (7), 1701–1736.

Alfano, M., Furgiuele, F., Leonardi, A., Maletta, C., Paulino, G.H., 2009. Mode I fracture of adhesive joints using tailored cohesive zone models. Int. J. Fract. 157 (1–2), 193–204.

Allaire, G., 1992. Homogenization and two-scale convergence. SIAM J. Math. Anal. 23 (6), 1482–1518.

Andrianov, I.V., Bolshakov, V.I., Danishevs'kyy, V.V., Weichert, D., 2008. Higher order asymptotic homogenization and wave propagation in periodic composite materials. Proc. R. Soc. A 464 (2093), 1181–1201.

Armstrong, S., Kuusi, T., Mourrat, J.-C., Prange, C., 2017. Quantitative analysis of boundary layers in periodic homogenization. Arch. Ration. Mech. Anal. 226 (2), 695–741.

Auriault, J.-L., Boutin, C., 2012. Long wavelength inner-resonance cut-off frequencies in elastic composite materials. Int. J. Solids Struct. 49 (23–24), 3269–3281.

Aymerich, F., Dore, F., Priolo, P., 2008. Prediction of impact-induced delamination in cross-ply composite laminates using cohesive interface elements. Compos. Sci. Technol. 68 (12), 2383–2390.

Ban, Y., Mi, C., 2020. Analytical solutions of a spherical nanoinhomogeneity under far-field unidirectional loading based on steigmann–ogden surface model. Math. Mech. Solids 25 (10), 1904–1923.

Barbagallo, G., Madeo, A., d'Agostino, M.V., Abreu, R., Ghiba, I.-D., Neff, P., 2017. Transparent anisotropy for the relaxed micromorphic model: Macroscopic consistency conditions and long wave length asymptotics. Int. J. Solids Struct. 120, 7–30.

Barenblatt, G.I., 1959. The formation of equilibrium cracks during brittle fracture. General ideas and hypotheses. Axially-symmetric cracks. J. Appl. Math. Mech. 23 (3), 622–636.

Barenblatt, G.I., 1962. The mathematical theory of equilibrium cracks in brittle fracture. Adv. Appl. Mech. 7 (C), 55–129.
Beneteau, C., 2021. Modèles homogénéisés enrichis en présence de bords: Analyse et traitement numérique (Ph.D. thesis). Institut Polytechnique de Paris.
Bensoussan, A., Lions, J.-L., Papanicolaou, G., 2011. Asymptotic Analysis for Periodic Structures. American Mathematical Society Providence, R.I, Providence, R.I.
Benveniste, Y., 2013. Models of thin interphases with variable moduli in plane-strain elasticity. Math. Mech. Solids 18 (2), 119–134.
Benveniste, Y., Miloh, T., 2001. Imperfect soft and stiff interfaces in two-dimensional elasticity. Mech. Mater. 33 (6), 309–323.
Bilal, O.R., Ballagi, D., Daraio, C., 2018. Architected lattices for simultaneous broadband attenuation of airborne sound and mechanical vibrations in all directions. Phys. Rev. A 10 (5).
Bordiga, G., Cabras, L., Piccolroaz, A., Bigoni, D., 2019. Prestress tuning of negative refraction and wave channeling from flexural sources. Appl. Phys. Lett. 114 (4).
Boutin, C., Rallu, A., Hans, S., 2014. Large scale modulation of high frequency waves in periodic elastic composites. J. Mech. Phys. Solids 70 (1), 362–381.
Bouvard, J.L., Chaboche, J.L., Feyel, F., Gallerneau, F., 2009. A cohesive zone model for fatigue and creep-fatigue crack growth in single crystal superalloys. Int. J. Fatigue 31 (5), 868–879.
Bövik, P., 1994. On the modelling of thin interface layers in elastic and acoustic scattering problems. Q. J. Mech. Appl. Math. 47 (1), 17–42.
Bückmann, T., Kadic, M., Schittny, R., Wegener, M., 2015. Mechanical cloak design by direct lattice transformation. Proc. Natl. Acad. Sci. USA 112 (16), 4930–4934.
Cakoni, F., Guzina, B.B., Moskow, S., 2016. On the homogenization of a scalar scattering problem for highly oscillating anisotropic media. SIAM J. Math. Anal. 48 (4), 2532–2560.
Cakoni, F., Guzina, B.B., Moskow, S., Pangburn, T., 2019. Scattering by a bounded highly oscillating periodic medium and the effect of boundary correctors. SIAM J. Appl. Math. 79 (4), 1448–1474.
Campilho, R., Banea, M.D., Neto, J., Da Silva, L., 2013. Modelling adhesive joints with cohesive zone models: Effect of the cohesive law shape of the adhesive layer. Int. J. Adhes. Adhes. 44, 48–56.
Celli, P., Yousefzadeh, B., Daraio, C., Gonella, S., 2019. Bandgap widening by disorder in rainbow metamaterials. Appl. Phys. Lett. 114 (9).
Chandra, N., 2002. Evaluation of interfacial fracture toughness using cohesive zone model. Composites A 33 (10), 1433–1447.
Charlotte, M., Laverne, J., Marigo, J.-J., 2006. Initiation of cracks with cohesive force models: a variational approach. Eur. J. Mech. A/Solids 25 (4), 649–669.
Chatzigeorgiou, G., Meraghni, F., Javili, A., 2017. Generalized interfacial energy and size effects in composites. J. Mech. Phys. Solids 106, 257–282.
Chen, T., Chiu, M.-S., Weng, C.-N., 2006. Derivation of the generalized Young-Laplace equation of curved interfaces in nanoscaled solids. J. Appl. Phys. 100 (7).
Chen, W., Fish, J., 2001. A dispersive model for wave propagation in periodic heterogeneous media based on homogenization with multiple spatial and temporal scales. J. Appl. Mech. Trans. ASME 68 (2), 153–161.
Chen, Q., Pindera, M.-J., 2020. Homogenization and localization of elastic-plastic nanoporous materials with gurtin-murdoch interfaces: An assessment of computational approaches. Int. J. Plast. 124, 42–70.
COMSOL, COMSOL Multiphysics® v. 6.0, COMSOL AB, Stockholm, Sweden.
Cornaggia, R., Lombard, B., 2023. A homogenized model accounting for dispersion, interfaces and source points for transient waves in 1D periodic media. ESAIM Math. Model. Numer. Anal. 57 (3), 1413–1444.
Craster, R.V., Kaplunov, J., Pichugin, A.V., 2010. High-frequency homogenization for periodic media. Proc. R. Soc. A 466 (2120), 2341–2362.
Cummer, S.A., Christensen, J., Alù, A., 2016. Controlling sound with acoustic metamaterials. Nat. Rev. Mater. 1.
Curie, P., 1894. Sur la symétrie dans les phénomènes physiques, symétrie d'un champ électrique et d'un champ magnétique. J. Phys. Théor. Appl. 3 (1), 393–415.
d'Agostino, M.V., Barbagallo, G., Ghiba, I.-D., Eidel, B., Neff, P., Madeo, A., 2020. Effective description of anisotropic wave dispersion in mechanical band-gap metamaterials via the relaxed micromorphic model. J. Elasticity 139 (2), 299–329.
dell'Isola, F., Madeo, A., Seppecher, P., 2009. Boundary conditions at fluid-permeable interfaces in porous media: A variational approach. Int. J. Solids Struct. 46 (17), 3150–3164.
dell'Isola, F., Romano, A., 1987. On the derivation of thermomechanical balance equations for continuous systems with a nonmaterial interface. Internat. J. Engrg. Sci. 25 (11–12), 1459–1468.
Demetriou, P., Rizzi, G., Madeo, A., 2023. Reduced relaxed micromorphic modeling of harmonically loaded metamaterial plates: investigating boundary effects in finite-size structures. Arch. Appl. Mech..
Demore, F., Rizzi, G., Collet, M., Neff, P., Madeo, A., 2022. Unfolding engineering metamaterials design: Relaxed micromorphic modeling of large-scale acoustic meta-structures. J. Mech. Phys. Solids 168.
Dimitri, R., Trullo, M., de Lorenzis, L., Zavarise, G., 2015. Coupled cohesive zone models for mixed-mode fracture: A comparative study. Eng. Fract. Mech. 148, 145–179.
Dingreville, R., Hallil, A., Berbenni, S., 2014. From coherent to incoherent mismatched interfaces: A generalized continuum formulation of surface stresses. J. Mech. Phys. Solids 72 (1), 40–60.
Dingreville, R., Qu, J., Mohammed Cherkaoui, 2005. Surface free energy and its effect on the elastic behavior of nano-sized particles, wires and films. J. Mech. Phys. Solids 53 (8), 1827–1854.
Duan, H.L., Wang, J., Huang, Z.P., Karihaloo, B.L., 2005. Size-dependent effective elastic constants of solids containing nano-inhomogeneities with interface stress. J. Mech. Phys. Solids 53 (7), 1574–1596.
Dugdale, D.S., 1960. Yielding of steel sheets containing slits. J. Mech. Phys. Solids 8 (2), 100–104.
El Sherbiny, M.G., Placidi, L., 2018. Discrete and continuous aspects of some metamaterial elastic structures with band gaps. Arch. Appl. Mech. 88 (10), 1725–1742.
England, A.H., 1966. An arc crack around a circular elastic inclusion. J. Appl. Mech. 33 (3), 637–640.
Espinosa, H.D., Dwivedi, S., Lu, H.-C., 2000. Modeling impact induced delamination of woven fiber reinforced composites with contact/cohesive laws. Comput. Methods Appl. Mech. Engrg. 183 (3–4), 259–290.
Fagerström, M., Larsson, R., 2006. Theory and numerics for finite deformation fracture modelling using strong discontinuities. Internat. J. Numer. Methods Engrg. 66 (6), 911–948.
Fan, H., Wang, G.F., 2003. Screw dislocation interacting with imperfect interface. Mech. Mater. 35 (10), 943–953.
Fedele, F., Suryanarayana, P., Yavari, A., 2023. On the effective dynamic mass of mechanical lattices with microstructure. J. Mech. Phys. Solids 179.
Firooz, S., Steinmann, P., Javili, A., 2021. Homogenization of composites with extended general interfaces: Comprehensive review and unified modeling. Appl. Mech. Rev. 73 (4).
Fried, E., Gurtin, M.E., 2007. Thermomechanics of the interface between a body and its environment. Contin. Mech. Thermodyn. 19 (5), 253–271.
Gasser, T.C., Holzapfel, G.A., 2003. Geometrically non-linear and consistently linearized embedded strong discontinuity models for 3D problems with an application to the dissection analysis of soft biological tissues. Comput. Methods Appl. Mech. Engrg. 192 (47–48), 5059–5098.
Gérard-Varet, D., Masmoudi, N., 2012. Homogenization and boundary layers. Acta Math. 209 (1), 133–178.
Geymonat, G., Krasucki, F., Lenci, S., 1999. Mathematical analysis of a bonded joint with a soft thin adhesive. Math. Mech. Solids 4 (2), 201–225.
Goh, H., Kallivokas, L.F., 2019. Inverse metamaterial design for controlling band gaps in scalar wave problems. Wave Motion 88, 85–105.
Guenneau, S., Movchan, A., Pétursson, G., Ramakrishna, S.A., 2007. Acoustic metamaterials for sound focusing and confinement. New J. Phys. 9.
Gurtin, M.E., Ian Murdoch, A., 1975. A continuum theory of elastic material surfaces. Arch. Ration. Mech. Anal. 57 (4), 291–323.

Hashin, Z., 2002. Thin interphase/imperfect interface in elasticity with application to coated fiber composites. J. Mech. Phys. Solids 50 (12), 2509–2537.
Hu, N., Zemba, Y., Okabe, T., Yan, C., Fukunaga, H., Elmarakbi, A.M., 2008. A new cohesive model for simulating delamination propagation in composite laminates under transverse loads. Mech. Mater. 40 (11), 920–935.
Huang, N.C., Korobeinik, M.Y., 2001. Interfacial debonding of a spherical inclusion embedded in an infinite medium under remote stress. Int. J. Fract. 107 (1), 11–30.
Ingraffea, A.R., Gerstk, W.H., Gergely, P., Saouma, V., 1984. Fracture mechanics of bond in reinforced concrete. J. Struct. Eng. (United States) 110 (4), 871–890.
Javili, A., Chatzigeorgiou, G., McBride, A.T., Steinmann, P., Linder, C., 2015. Computational homogenization of nano-materials accounting for size effects via surface elasticity. GAMM-Mitt. 38 (2), 285–312.
Javili, A., McBride, A., Steinmann, P., 2013. Thermomechanics of solids with lower-dimensional energetics: On the importance of surface, interface, and curve structures at the nanoscale. A unifying review. Appl. Mech. Rev. 65 (1).
Javili, A., Steinmann, P., Mosler, J., 2017. Micro-to-macro transition accounting for general imperfect interfaces. Comput. Methods Appl. Mech. Engrg. 317, 274–317.
Josien, M., 2019. Some quantitative homogenization results in a simple case of interface. Comm. Partial Differential Equations 44 (10), 907–939.
Kaina, N., Causier, A., Bourlier, Y., Fink, M., Berthelot, T., Lerosey, G., 2017. Slow waves in locally resonant metamaterials line defect waveguides. Sci. Rep. 7 (1).
Kawashita, L.F., Hallett, S.R., 2012. A crack tip tracking algorithm for cohesive interface element analysis of fatigue delamination propagation in composite materials. Int. J. Solids Struct. 49 (21), 2898–2913.
Klarbring, A., 1991. Derivation of a model of adhesively bonded joints by the asymptotic expansion method. Internat. J. Engrg. Sci. 29 (4), 493–512.
Klarbring, A., Movchan, A.B., 1998. Asymptotic modelling of adhesive joints. Mech. Mater. 28 (1–4), 137–145.
Koutsianitis, P.I., Tairidis, G.K., Drosopoulos, G.A., Stavroulakis, G.E., 2019. Conventional and star-shaped auxetic materials for the creation of band gaps. Arch. Appl. Mech. 89 (12), 2545–2562.
Le, T.-T., 2020. Multiscale analysis of elastic properties of nano-reinforced materials exhibiting surface effects. Application for determination of effective shear modulus. J. Composites Sci. 4 (4).
Li, S., Thouless, M.D., Waas, A.M., Schroeder, J.A., Zavattieri, P.D., 2005. Use of mode-i cohesive-zone models to describe the fracture of an adhesively-bonded polymer-matrix composite. Compos. Sci. Technol. 65 (2), 281–293.
Liu, P.F., Islam, M.M., 2013. A nonlinear cohesive model for mixed-mode delamination of composite laminates. Compos. Struct. 106, 47–56.
Liu, L., Sridhar, A., Geers, M., Kouznetsova, V.G., 2021. Computational homogenization of locally resonant acoustic metamaterial panels towards enriched continuum beam/shell structures. Comput. Methods Appl. Mech. Engrg. 387.
Liu, Z., Zhang, X., Mao, Y., Zhu, Y.Y., Yang, Z., Chan, C.T., Sheng, P., 2000. Locally resonant sonic materials. Science 289 (5485), 1734–1736.
Lustig, B., Elbaz, G., Muhafra, A., Shmuel, G., 2019. Anomalous energy transport in laminates with exceptional points. J. Mech. Phys. Solids 133.
Madeo, A., Neff, P., Ghiba, I.D., Placidi, L., Rosi, G., 2015. Wave propagation in relaxed micromorphic continua: modeling metamaterials with frequency band-gaps. Contin. Mech. Thermodyn. 27 (4–5), 551–570.
Marigo, J.-J., Maurel, A., 2016. Two-scale homogenization to determine effective parameters of thin metallic-structured films. Proc. R. Soc. A 472 (2192).
Marigo, J.-J., Maurel, A., 2017. Second order homogenization of subwavelength stratified media including finite size effect. SIAM J. Appl. Math. 77 (2), 721–743.
Maurel, A., Marigo, J.-J., 2018. Sensitivity of a dielectric layered structure on a scale below the periodicity: A fully local homogenized model. Phys. Rev. B 98 (2).
Miniaci, M., Pal, R.K., Manna, R., Ruzzene, M., 2019. Valley-based splitting of topologically protected helical waves in elastic plates. Phys. Rev. B 100 (2).
Misseroni, D., Colquitt, D.J., Movchan, A.B., Movchan, N.V., Jones, I.S., 2016. Cymatics for the cloaking of flexural vibrations in a structured plate. Sci. Rep. 6.
Misseroni, D., Movchan, A.B., Bigoni, D., 2019. Omnidirectional flexural invisibility of multiple interacting voids in vibrating elastic plates. Proc. R. Soc. A 475 (2229).
Moeckel, G.P., 1975. Thermodynamics of an interface. Arch. Ration. Mech. Anal. 57 (3), 255–280.
Mogilevskaya, S.G., Crouch, S.L., Stolarski, H.K., 2008. Multiple interacting circular nano-inhomogeneities with surface/interface effects. J. Mech. Phys. Solids 56 (6), 2298–2327.
Monchiet, V., Bonnet, G., 2010. Interfacial models in viscoplastic composites materials. Internat. J. Engrg. Sci. 48 (12), 1762–1768.
Mori, T., Mura, T., 1987. Blocking effect of inclusions on grain boundary sliding; spherical grain approximation. J. Mech. Phys. Solids 35 (5), 631–641.
Morini, L., Eyzat, Y., Gei, M., 2019. Negative refraction in quasicrystalline multilayered metamaterials. J. Mech. Phys. Solids 124, 282–298.
Moskow, S., Vogelius, M., 1997. First-order corrections to the homogenised eigenvalues of a periodic composite medium. a convergence proof. R. Soc. Edinb. Proc. A 127 (6), 1263–1299.
Mosler, J., Scheider, I., 2011. A thermodynamically and variationally consistent class of damage-type cohesive models. J. Mech. Phys. Solids 59 (8), 1647–1668.
Mubashar, A., Ashcroft, I.A., Critchlow, G.W., Crocombe, A.D., 2011. Strength prediction of adhesive joints after cyclic moisture conditioning using a cohesive zone model. Eng. Fract. Mech. 78 (16), 2746–2760.
Murdoch, A.I., 1976. A thermodynamical theory of elastic material interfaces. Q. J. Mech. Appl. Math. 29 (3), 245–275.
Needleman, A., 1987. A continuum model for void nucleation by inclusion debonding. J. Appl. Mech. Trans. ASME 54 (3), 525–531.
Neff, P., Eidel, B., d'Agostino, M.V., Madeo, A., 2020. Identification of scale-independent material parameters in the relaxed micromorphic model through model-adapted first order homogenization. J. Elasticity 139 (2), 269–298.
Neff, P., Ghiba, I.D., Lazar, M., Madeo, A., 2015. The relaxed linear micromorphic continuum: well-posedness of the static problem and relations to the gauge theory of dislocations. Quart. J. Mech. Appl. Math. 68 (1), 53–84.
Neff, P., Ghiba, I.-D., Madeo, A., Placidi, L., Rosi, G., 2014. A unifying perspective: the relaxed linear micromorphic continuum. Contin. Mech. Thermodyn. 26 (5), 639–681.
Norris, A.N., Amirkulova, F.A., Parnell, W.J., 2014. Active elastodynamic cloaking. Math. Mech. Solids 19 (6), 603–625.
Ortiz, M., Pandolfi, A., 1999. Finite-deformation irreversible cohesive elements for three-dimensional crack-propagation analysis. Internat. J. Numer. Methods Engrg. 44 (9), 1267–1282.
Ottosen, N.S., Ristinmaa, M., Mosler, J., 2016. Framework for non-coherent interface models at finite displacement jumps and finite strains. J. Mech. Phys. Solids 90, 124–141.
Park, K., Paulino, G.H., 2011. Cohesive zone models: A critical review of traction-separation relationships across fracture surfaces. Appl. Mech. Rev. 64 (6).
Park, K., Paulino, G.H., Roesler, J.R., 2009. A unified potential-based cohesive model of mixed-mode fracture. J. Mech. Phys. Solids 57 (6), 891–908.
Parrinello, F., Marannano, G., Borino, G., 2016. A thermodynamically consistent cohesive-frictional interface model for mixed mode delamination. Eng. Fract. Mech. 153, 61–79.
Perez Ramirez, L.A., Rizzi, G., Madeo, A., 2023. Multi-element metamaterial's design through the relaxed micromorphic model. In: Altenbach, H., Berezovski, A., dell'Isola, F., Porubov, A. (Eds.), Sixty Shades of Generalized Continua: Dedicated To the 60th Birthday of Prof. Victor a. Eremeyev. Springer International Publishing, Cham, pp. 579–600.
Pezzotta, M., Zhang, Z.L., Jensen, M., Grande, T., Einarsrud, M.-A., 2008. Cohesive zone modeling of grain boundary microcracking induced by thermal anisotropy in titanium diboride ceramics. Comput. Mater. Sci. 43 (3), 440–449.
Reinoso, J., Paggi, M., Blázquez, A., 2017. A nonlinear finite thickness cohesive interface element for modeling delamination in fibre-reinforced composite laminates. Composites B 109, 116–128.

Rizzi, G., Collet, M., Demore, F., Eidel, B., Neff, P., Madeo, A., 2021. Exploring metamaterials' structures through the relaxed micromorphic model: Switching an acoustic screen into an acoustic absorber. Front. Mater. 7.
Rizzi, G., d'Agostino, M.V., Neff, P., Madeo, A., 2022a. Boundary and interface conditions in the relaxed micromorphic model: Exploring finite-size metastructures for elastic wave control. Math. Mech. Solids 27 (6), 1053–1068.
Rizzi, G., Neff, P., Madeo, A., 2022b. Metamaterial shields for inner protection and outer tuning through a relaxed micromorphic approach. Phil. Trans. R. Soc. A 380 (2231).
Rizzi, G., Tallarico, D., Neff, P., Madeo, A., 2022c. Towards the conception of complex engineering meta-structures: Relaxed-micromorphic modelling of low-frequency mechanical diodes/high-frequency screens. Wave Motion 113.
Roe, K.L., Siegmund, T., 2003. An irreversible cohesive zone model for interface fatigue crack growth simulation. Eng. Fract. Mech. 70 (2), 209–232.
Rossi, M., Veber, D., Gei, M., 2020. Numerical assessment of the performance of elastic cloaks for transient flexural waves. Front. Mater. 7.
Sharma, P., 2004. Size-dependent elastic fields of embedded inclusions in isotropic chiral solids. Int. J. Solids Struct. 41 (22–23), 6317–6333.
Sharma, P., Ganti, S., 2004. Size-dependent eshelby's tensor for embedded nano-inclusions incorporating surface/interface energies. J. Appl. Mech. 71 (5), 663–671.
Sharma, P., Ganti, S., Bhate, N., 2003. Effect of surfaces on the size-dependent elastic state of nano-inhomogeneities. Appl. Phys. Lett. 82 (4), 535–537.
Sharma, P., Wheeler, L.T., 2007. Size-dependent elastic state of ellipsoidal nano-inclusions incorporating surface/interface tension. J. Appl. Mech. 74 (3), 447–454.
Shih, G.C., Ebert, L.J., 1987. Theoretical modelling of the effect of the interfacial shear strength on the longitudinal tensile strength of unidirectional composites. J. Compos. Mater. 21 (3), 207–224.
Shuttleworth, R., 1950. The surface tension of solids. Proc. Phys. Soc. Section A 63 (5), 444–457.
Spannraft, L., Possart, G., Steinmann, P., Mergheim, J., 2022. Generalized interfaces enabling macroscopic modeling of structural adhesives and their failure. Forces Mech. 9, 100137.
Sridhar, A., Kouznetsova, V.G., Geers, M., 2016. Homogenization of locally resonant acoustic metamaterials towards an emergent enriched continuum. Comput. Mech. 57 (3), 423–435.
Srivastava, A., 2016. Metamaterial properties of periodic laminates. J. Mech. Phys. Solids 96, 252–263.
Sun, C.T., Jin, Z.-H., 2006. Modeling of composite fracture using cohesive zone and bridging models. Compos. Sci. Technol. 66 (10), 1297–1302.
Tallarico, D., Trevisan, A., Movchan, N.V., Movchan, A.B., 2017. Edge waves and localization in lattices containing tilted resonators. Front. Mater. 4.
Touboul, M., Pham, K., Maurel, A., Marigo, J.-J., Lombard, B., Bellis, C., 2020. Effective resonant model and simulations in the time-domain of wave scattering from a periodic row of highly-contrasted inclusions. J. Elasticity 142 (1), 53–82.
Tvergaard, V., Hutchinson, J.W., 1993. The influence of plasticity on mixed mode interface toughness. J. Mech. Phys. Solids 41 (6), 1119–1135.
Tvergaard, V., Hutchinson, J.W., 1996. Effect of strain-dependent cohesive zone model on predictions of crack growth resistance. Int. J. Solids Struct. 33 (20–22), 3297–3308.
van den Bosch, M.J., Schreurs, P., Geers, M., 2006. An improved description of the exponential xu and needleman cohesive zone law for mixed-mode decohesion. Eng. Fract. Mech. 73 (9), 1220–1234.
Vinoles, V., 2016. Interface problems with metamaterials: modelling, analysis and simulations (Ph.D. thesis). ENSTA Paris-Saclay.
Vinoles, V., 2019. Wave propagation in periodic media : mathematical analysis and numerical simulation (Habilitation thesis). ENSTA Paris-Saclay.
Voss, J., Rizzi, G., Neff, P., Madeo, A., 2023. Modeling a labyrinthine acoustic metamaterial through an inertia-augmented relaxed micromorphic approach. Math. Mech. Solids 28 (10), 2177–2201.
Wang, P., Casadei, F., Shan, S., Weaver, J.C., Bertoldi, K., 2014. Harnessing buckling to design tunable locally resonant acoustic metamaterials. Phys. Rev. Lett. 113 (1).
Wang, Y.-F., Wang, T.-T., Liang, J.-W., Wang, Y.-S., Laude, V., 2018. Channeled spectrum in the transmission of phononic crystal waveguides. J. Sound Vib. 437, 410–421.
Wei, Y., Hutchinson, J.W., 1998. Interface strength, work of adhesion and plasticity in the peel test. Int. J. Fract. 93 (1–4), 315–333.
Wei, Y., Hutchinson, J.W., 1999. Models of interface separation accompanied by plastic dissipation at multiple scales. Int. J. Fract. 95 (1–4), 1–17.
Willis, J.R., 2011. Effective constitutive relations for waves in composites and metamaterials. Proc. R. Soc. A 467 (2131), 1865–1879.
Willis, J.R., 2012. The construction of effective relations for waves in a composite. C. R. Mecanique 340 (4–5), 181–192.
Willis, J.R., 2016. Negative refraction in a laminate. J. Mech. Phys. Solids 97, 10–18.
Wulfinghoff, S., 2017. A generalized cohesive zone model and a grain boundary yield criterion for gradient plasticity derived from surface- and interface-related arguments. Int. J. Plast. 92, 57–78.
Xu, X.-P., Needleman, A., 1994. Numerical simulations of fast crack growth in brittle solids. J. Mech. Phys. Solids 42 (9), 1397–1434.
Xu, C., Siegmund, T., Ramani, K., 2003. Rate-dependent crack growth in adhesives: I. Modeling approach. Int. J. Adhes. Adhes. 23 (1), 9–13.
Yang, F., 2004. Size-dependent effective modulus of elastic composite materials: Spherical nanocavities at dilute concentrations. J. Appl. Phys. 95 (7), 3516–3520.
Yang, B., Mall, S., Ravi-Chandar, K., 2001. A cohesive zone model for fatigue crack growth in quasibrittle materials. Int. J. Solids Struct. 38 (22–23), 3927–3944.
Yvonnet, J., Quang, H.L., He, Q.-C., 2008. An XFEM/level set approach to modelling surface/interface effects and to computing the size-dependent effective properties of nanocomposites. Comput. Mech. 42 (1), 119–131.
Zemlyanova, A.Y., Mogilevskaya, S.G., 2018. On spherical inhomogeneity with steigmann-ogden interface. J. Appl. Mech. Trans. ASME 85 (12).
Zhang, L., Wang, J., 2009. A generalized cohesive zone model of the peel test for pressure-sensitive adhesives. Int. J. Adhes. Adhes. 29 (3), 217–224.
Zhu, R., Liu, X.N., Huang, G.L., 2015. Study of anomalous wave propagation and reflection in semi-infinite elastic metamaterials. Wave Motion 55, 73–83.